



2,2'-Ethylenebis(1,3-dithiane) as polydentate m2-, m4- and m5-assembling ligand for the construction of sulphur-rich Cu(I), Hg(II) and heterometallic Cu(I)/Hg(II) coordination polymers featuring uncommon network architectures

Lydie Viau, Michael Knorr, Lena Knauer, Lukas Brieger, Carsten Strohman

► To cite this version:

Lydie Viau, Michael Knorr, Lena Knauer, Lukas Brieger, Carsten Strohman. 2,2'-Ethylenebis(1,3-dithiane) as polydentate m2-, m4- and m5-assembling ligand for the construction of sulphur-rich Cu(I), Hg(II) and heterometallic Cu(I)/Hg(II) coordination polymers featuring uncommon network architectures. Dalton Transactions, 2022, 51 (19), pp.7581-7606. 10.1039/D2DT00800A . hal-03647065

HAL Id: hal-03647065

<https://hal.science/hal-03647065>

Submitted on 8 Nov 2022

HAL is a multi-disciplinary open access archive for the deposit and dissemination of scientific research documents, whether they are published or not. The documents may come from teaching and research institutions in France or abroad, or from public or private research centers.

L'archive ouverte pluridisciplinaire **HAL**, est destinée au dépôt et à la diffusion de documents scientifiques de niveau recherche, publiés ou non, émanant des établissements d'enseignement et de recherche français ou étrangers, des laboratoires publics ou privés.

2,2'-Ethylenebis(1,3-dithiane) as polydentate μ_2 -, μ_4 - and μ_5 -assembling ligand for the construction of sulphur-rich Cu(I), Hg(II) and heterometallic Cu(I)/Hg(II) coordination polymers featuring uncommon network architectures

Lydie Viau,^{*,[a]} Michael Knorr,^{*,[a]} Lena Knauer,^[b] Lukas Brieger,^[b] and Carsten Strohmann^{*,[b]}

*a) Institut UTINAM UMR CNRS 6213, Université Bourgogne Franche-Comté, F-25030 Besançon, France. Corresponding authors: E-mail: michael.knorr@univ-fcomte.fr; lydie.viau@univ-fcomte.fr
b) Anorganische Chemie, Technische Universität Dortmund, Otto-Hahn-Straße 6, D-44227 Dortmund, Germany. E-mail: carsten.strohmanna@tu-dortmund.de*

ABSTRACT

With the aim to elaborate novel and inexpensive sulphur-rich materials featuring unusual network architectures, the coordination chemistry of the tetradentate thiaheterocycle 1,2-di(1,3-dithian-2-yl)ethane **L1** ligand toward CuX and HgX₂ salts was investigated. When **L1** is reacted with CuI in a 1:1 ratio, a two-dimensional CP [$\{\text{Cu}(\mu_2\text{-I})_2\text{Cu}\}(\mu_2\text{-L1})_n$] (**CP1**) is formed, in which two out of four S atoms of **L1** remain non-coordinated. A particularity is the occurrence of three different type of $[\text{Cu}(\mu_2\text{-I})_2\text{Cu}]$ rhomboids as SBU (Secondary Building Unit), which differ in the Cu...Cu distances. Upon treatment of **L1** with CuI in a 1:2 ratio, [$\{\text{Cu}(\mu_2\text{-I})_2\text{Cu}\}(\mu_4\text{-L1})_n$] (**CP2**) is obtained, in which each S atom of **L1** coordinates to one copper centre forming a 2D layer. Contrary to **CP1**, **CP2** contains a single type of $[\text{Cu}(\mu_2\text{-I})_2\text{Cu}]$ SBU, but with a particular short Cu...Cu bond length of 2.6132(9) Å. Raising the ligand-to-CuI ratio to 1:4 affords the 2D material [$\{\text{Cu}(\mu_4\text{-I})(\mu_2\text{-I})\text{Cu}\}_2(\mu_4\text{-L1})_n$] (**CP3**), in which $[\text{Cu}(\mu_4\text{-I})(\mu_2\text{-I})\text{Cu}]_n$ ribbons are interconnected through μ_4 -bridging **L1** ligands. Upon reaction of **L1** with CuBr in a 1:2 ratio, a 2D CP [$\{\text{Cu}(\mu_2\text{-Br})\}_2(\mu_4\text{-L1})_n$] (**CP4**) is formed, in which the Cu atoms are bridged by a single μ_2 -Br ligand giving rise to $[\text{Cu}(\mu_2\text{-Br})\text{Cu}]_n$ ribbons. Employing a 1:3 ratio, a 1D ribbon [$\{\text{Cu}(\mu_2\text{-Br})\}_3(\text{MeCN})(\mu_4\text{-L1})_n$] (**CP5**) is generated, which five out of the six different copper atoms present a tetrahedral geometry, while the sixth one is only three-coordinated. **CP5** also presents two different **L1** ligands that differ by the coordination mode of the sulphur atoms (S acting as 2 or as 4 electron-donor). With CuCl, a 2D network [$\{\text{Cu}(\mu_2\text{-Cl})_2\text{Cu}\}(\mu_4\text{-L1})_n$] (**CP6**) is generated.

L1 coordinates also on HgX₂ salts to yield CPs whose architecture depends on the ligand-to-metal ratio. The meander-shaped 1D CP [(HgI₂)(μ₂-**L1**)]_n (**CP7**) and the linear 1D ribbons of **CP8** and **CP11** [(HgX₂)(μ₂-**L1**)]_n (X = Br, Cl) result from treatment with **L1** in a 1:1 ratio. In the case of HgBr₂, using a 2:1 metal-to-ligand ratio, 1D polymeric [{BrHg(μ₂-Br)₂HgBr}(μ₂-**L1**)] (**CP9**) is produced. HgI₂ and HgBr₂ have also been reacted with 2-methyl-1,3-dithiane **L2** yielding the molecular complexes [{IHg(μ₂-I)₂HgI}(κ¹-**L2**)₂] (**D1**) and [HgBr₂(κ¹-**L2**)₂] (**M1**). A heterometallic 1D material [{IHg(μ₂-I)₂HgI(μ₂-I)₂{Cu(MeCN)₂}₂(μ₂-**L1**)]_n (**CP12**) results from treatment of **CP1** with HgI₂.

Introduction

Coordination polymers (CPs), especially those formed by assembly of inexpensive copper(I) salts with organosulphur ligands such as thioether R-S-R and thiolates R-S⁻ present interesting structural and photophysical properties.¹ Complexes, CPs and even MOFs with different dimensionality (0D to 3D) and secondary building units (SBUs) could be constructed depending on the nature of the ligands, the metal-to-ligand ratio and the experimental conditions (solvent, temperature etc.). Beside their interest in crystal engineering, these materials have also found applications in sensing, optoelectronics² and catalysis.³ They have also been used as precursors to prepare materials *i.e.* γ -CuI nanocrystals⁴ or as a precursor for CuI-based thermoelectric composites, exhibiting a moderate to high Seebeck coefficient (543–1308 $\mu\text{V K}^{-1}$) at elevated temperature.⁵ Stretchable, luminescent and self-healing hybrid films were obtained using polymers bearing thioethers functions allowing further coordination to copper iodide.⁶

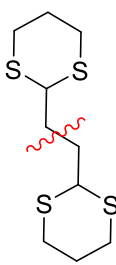
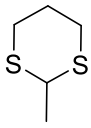
Several research groups, including ours, have been interested in the formation of various CPs by reacting copper(I) salts with different mono or dithioether ligands. Though the results of the self-assembly process are difficult to predict, Schlachter *et al* have recently reviewed on networks built upon chalcogenoether and chalcogenone assemblies, providing some very interesting trends based on the architecture of the assembling ligands and the nature of the halide.⁷ In particular, for sensing applications, the design of porous 3D CP materials plays a crucial role. One may expect that the construction of high-dimensional CPs and MOFs is favoured using tridentate or tetradentate ligands. Different polydentate phosphine- and amine-based ligands have been used for the assembly of Cu(I) complexes and CPs, however examples of Cu(I)-based CPs obtained using polydentate organosulfur ligands are much scarce. One of the first example is the coordination of the tridentate thioether ligand MeSi(CH₂SMe)₃ with CuX salts that led to the formation of 1D CPs.⁸ In 2001, Brooks *et al.* reported the coordination of [12]aneS₄ (1,4,7,10-tetrathiacyclododecane) or [16]aneS₄ (1,5,9,13-tetrathiacyclohexadecane) with CuBr or CuI leading to the formation of either discrete molecular entities or CPs with 2D or 3D structures containing rhomboid dimers as SBU when the metal to ligand ratio is increased.⁹ 3D CuI-based CPs containing the calix[4]-bis-thiacrown were reported by Lee *et al.* in 2008¹⁰ and 2D CPs were obtained by assembly of CuI with *p*-tert-

butylthiacalix[4]-arene.¹¹ The cyclophane derivative 2,11,20,29-tetrathia-dodecahydro[3.3.3.3]cyclophane reacts with CuI in MeCN in a 1:1 molar ratio to generate a 3D CP built upon rhomboid dimers as SBUs.¹² In a collaborative work, our group has reported on the network assembly of octadentate thioether-decorated octasilsesquioxanes with CuI salts under mild conditions yielding 3D POSS-based CPs incorporating dinuclear or close-cubanes SBUs.¹³ The tetradentate thioether functionalized silanes Si(CH₂SR)₄ (R = Me or Ph) was found to react with HgBr₂ yielding 1D CPs, where HgBr₂ moieties are connected by doubly bidentate chelating thioether ligands.¹⁴

Five-, six- and seven-membered dithiaheterocycles have been used in the past by several groups as ligand in coordination chemistry.^{15, 16} In the case of 1,3-dithianes, it has been demonstrated that the parent compound 1,3-dithiacyclohexane may be coordinated as mono- and bidentate ligand to a series of early and late transition metal complexes. Several CPs have been built up by treatment of 1,3-dithiane with AgNO₃, AgBF₄ and AgPF₆, respectively.¹⁷ Keller and Knaust reacted [Cu(MeCN)₄]BF₄ with that dithiaheterocycle and obtained four coordination networks depending on metal-to-ligand ratio and solvent conditions used.¹⁸ In the context of our research work on the coordination chemistry of dithiolanes and dithianes with Cu(I) salts, we have recently investigated in an exhaustive manner the possibility to construct coordination polymers using both parent 1,3-dithiane and a series of derivatives substituted at the 2-position such as 2-isobutyl-1,3-dithiane, 2-Me₃Si-1,3-dithiane, 2-phenyl-1,3-dithiane, 2-ferrocenyl-1,3-dithiane and 2-methyl-1,3-dithiane.¹⁹⁻²³ Notably with the latter ligand, we demonstrated that CPs with uncommon architectures and dimensionalities ranging from discrete 0D to 3D can be obtained, in function of the nature of CuX (X = Cl, Br, I, CN) and the metal-to-ligand ratio. We highlighted furthermore that with CuI an original 3D network [$\{Cu_8(\mu_3-I)_8\}(\mu_2$ -2-methyl-1,3-dithiane)₄]_n can be constructed, which incorporates strongly luminescent and unprecedented octanuclear Cu₈I₈S₈ clusters as SBUs (Secondary Building Units).²¹ The original idea of the present work was to try to obtain 3D CPs showing interesting structural and photophysical properties. For this, we raised the number of available S-donor sites from two to four using 2,2'-ethylenebis(1,3-dithiane) **L1** ligand. We herein present our results on the coordination of **L1** *vis-à-vis* CuX salts under varying reaction conditions. This cyclic bisdithioacetal, which has hitherto never been explored as ligand system, was

chosen due to its structural resemblance with 2-methyl-1,3-dithiane **L2**, since it combines formally two $C_4H_7S_2CH_2$ moieties (Chart 1). This investigation on the coordination chemistry of **L1** has been extended towards other soft metal salts, namely $HgBr_2$ and HgI_2 and we present the crystal structures of all novel CPs including that of **L1**. For comparison, HgI_2 and $HgBr_2$ were also treated with **L2** and the resulting materials were characterized by means of single-crystal X-ray diffraction studies. Exploiting the presence of numerous uncoordinated *S*-donor sites in some of our sulphur-rich CuX materials presented in this work, we also succeed to use one example as precursor for a heterometallic HgI_2CuI array and present here the crystal structure of the of the unique 1D ribbon of $[\{ IHg(\mu_2-I)_2HgI(\mu_2-I)_2 \{ Cu(MeCN)_2 \}_2 (\mu_2-L1) \}]_n$ (**CP12**).

Chart 1. Overview of the investigated dithiane ligands and CPs including those previously published

Ligand	Metal	X (Ligand:Metal Ratio)	CPs	SBU	Ligand L1/L2 hapticity	Dimensi onality
 L1	Cu	I (1:1)	CP1	$Cu(\mu_2-I)_2Cu$	μ_2	2D
		I (1:2)	CP2	$Cu(\mu_2-I)_2Cu$	μ_4	2D
		I (1:4)	CP3	$Cu_2(\mu_4-I)(\mu_2-I)$	μ_4	2D
		Br (1:2)	CP4	$Cu(\mu_2-Br)_2Cu$	μ_4	2D
		Br (1:3)	CP5	$Cu(\mu_2-Br)_3(MeCN)$	μ_4 and μ_5	1D
		Cl (1:2)	CP6	$Cu(\mu_2-Cl)_2Cu$	μ_4	2D
	Hg	I (1:1)	CP7	HgI_2	μ_2	1D
		Br (1:1)	CP8	$HgBr_2$	μ_2	1D
		Br (1:2)	CP9	$Br_2Hg_2(\mu_2-Br)_2$	μ_2	1D
		Cl (1:1)	CP11	$HgCl_2$	μ_2	1D
	Cu+Hg	I (1:1:1)	CP12	$IHg(\mu_2-I)(\mu_2-I)\{ Cu(MeCN)_2 \}$	μ_2	1D
 L2	Cu	I (1:1)	Ref ²¹	$Cu(\mu_2-I)_2Cu$	μ_2	1D or
		I (1:2)	Ref ²¹	$Cu_8(\mu_3-I)_8$	μ_2	2D
		Br (1:1)	Ref ²²	$Cu(\mu_2-Br)_2Cu$	μ_2	3D
		Cl (1:1)	Ref ²²	$Cu(\mu_2-Cl)_2Cu$	μ_2	1D
	Hg	I (1:1)	D1	$IHg(\mu_2-I)$	κ^1	0D
		Br (1:1)	M1	$HgBr_2$	κ^1	0D
		Br (1:2)	CP10	$HgBr_2$	μ_2	1D

Results and discussion

Structural Characterization of L1

The ethylene-bridged compound 2,2'-ethylenebis(1,3-dithiane) **L1** was first synthesized in 1968 by *Seebach et al.* via treatment of 2,5-dimethoxytetrahydrofuran with 1,3-propanethiol.²⁴ **L1** is also an interesting ligand in organic chemistry and is used as starting material for the preparation of *cis*-jasnone or the preparation of γ -diketones, 2,5-bis(trialkylsilyl)furans and 2,6-bis(trialkylsilyl)-4*H*-pyrans.²⁵ Except for the parent compound 1,3-dithiane and 2-phenyl-1,3-dithiane, most other 1,3-dithiane are liquids at ambient temperature. Therefore, the structural database is quite limited. Since **L1** is also a solid, we recrystallized a commercial sample from hot EtOH and obtained a crystalline product suitable for an X-ray analysis. The molecular structure of this sulphur-rich compound is shown in Fig. 1, the crystallographic refinement data are gathered in Table S1. The six-membered dithiane-heterocycle of **L1** adopts the chair conformation encountered also in 2-phenyl-1,3-dithiane.²⁶ Like the phenyl group in the latter thiaheterocycle, the C2 atom of methylene group linking the two six-membered rings occupies the equatorial position. The mid-point of the C2–C2# bond constitutes the symmetry centre of the two identical moieties. The bond lengths and angles in **L1** are normal for this kind of molecules and deserve no further comments.

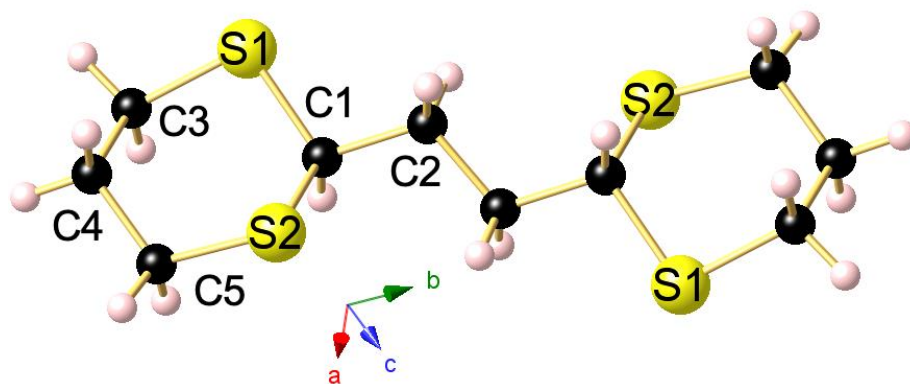


Figure 1. Molecular structure of **L1**. Selected bond lengths (Å) and angles (°): C1–S1 1.8134(6), C1–S2 1.8139(7), C3–S1 1.819(7), C5–S2 1.8111(7), C1–C2 1.5275(9), C2–C2# 1.5301(13); S2–C1–S1 112.72(3), C3–S1–C1 98.75(3), C5–S2–C1 99.00(3), S1–C1–C2 108.15(4), S2–C1–C2 110.05(4), C1–C2–C2# 113.12(7), C3–C4–C5 112.86(6).

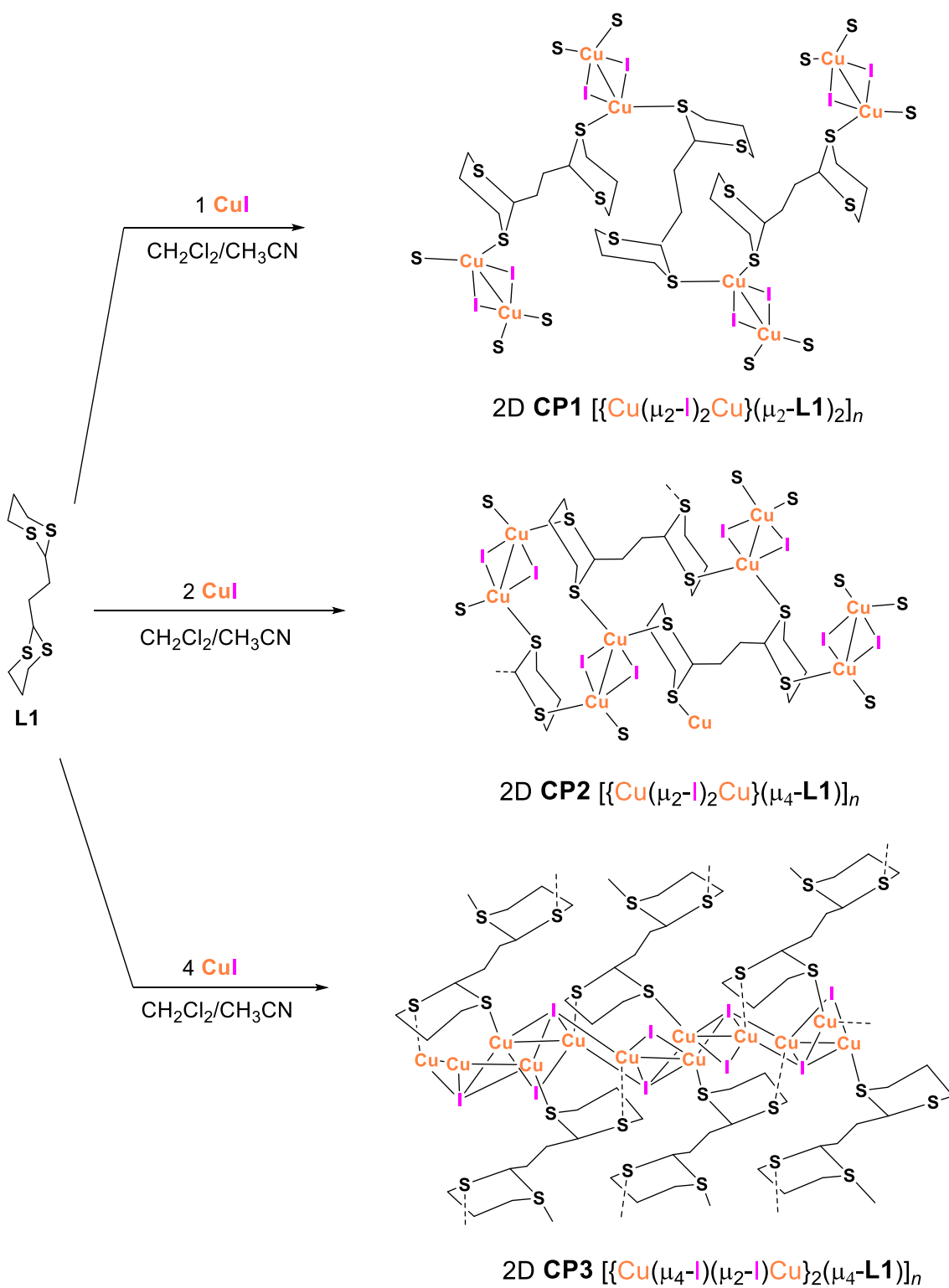
Reaction of **L1** with CuI

The reaction of CuI with 1 equivalent of **L1** in a CH₂Cl₂/MeCN mixture affords **CP1** in 89% yield (Scheme 1). X-ray suitable single crystals crystallizing in the monoclinic space group P2₁/n were obtained from dissolution of solid samples in hot MeCN. In **CP1**, two sulphur atoms of **L1** remain non-coordinated (Figures 2 and S1). Noteworthy, **CP1** also contains three different types of rhomboids featuring different metric parameters. Within the Cu₂-Cu₂ SBU, the Cu–Cu distance is the shortest ($d_{\text{Cu2}\cdots\text{Cu2}}$ 2.8399(5) Å) and reaches 2.8820(4) Å within the Cu₁-Cu₄ SBU and 2.9436(5) Å in the Cu₃-Cu₃ SBU. Examples of CPs incorporating different types of Cu(μ₂-X)₂Cu rhomboids within the same array are quite rare. We have already encountered such observations in two cases: a 1D CP [$\{\text{Cu}(\mu_2\text{-Br})_2\text{Cu}\}(\mu\text{-}p\text{-MeC}_6\text{H}_4\text{SCH}_2\text{C}\equiv\text{CCH}_2\text{SC}_6\text{H}_4\text{Me-}p)_2]_n$, showing two different type of Cu(μ₂-Br)₂Cu SBUs with Δ(Cu–Cu 0.0356 Å) and in a 1D ribbon [$\{\text{Cu}(\mu_2\text{-I})_2\text{Cu}\}(\text{MeCN})_2(\mu_2\text{-2-phenyl-1,3-dithiane})]_n$ that possesses also two different type of Cu(μ₂-I)₂Cu SBUs with Δ(Cu–Cu 0.0489 Å).^{22, 27} The difference in the Cu–Cu distance in **CP1** is clearly much more significant with Δ(Cu–Cu 0.1037 Å). To our knowledge, the occurrence of three different rhomboids in a network is unprecedented.

When the reaction was performed in a 1:2 ratio, the resulting colourless product was crystallographically characterized as a 2D CP of composition [$\{\text{Cu}(\mu_2\text{-I})_2\text{Cu}\}(\mu_4\text{-L1})]_n$ (**CP2**) (Scheme 1). Likewise, as in **CP1**, the **CP2** network is also built upon Cu(μ₂-I)₂Cu rhomboids but unlike in **CP1**, all sulphur atoms are now coordinated in a μ-1κS:2κS:3κS:4κS coordination mode (Figures 3 and S2). Both copper(I) ions of the central dimeric Cu₂I₂ motif possess the same fourfold coordination to two iodine and two sulphur atoms, respectively, resulting in a distorted tetrahedral geometry. A more striking observation is the short Cu–Cu distance of 2.6131(9) Å. This distance is much shorter than what was already observed for other 2D CPs containing the S₂Cu₂I₂S₂ motif obtained by the reaction of CuI with the parent 2-methyldithiane **L2** ($d_{\text{Cu}\cdots\text{Cu}}$ 2.7664 Å),²¹ the bis(benzylthio)butane ($d_{\text{Cu}\cdots\text{Cu}}$ 2.796 Å)²⁸ and 1,4-bis(phenylthio)but-2-ene ligands ($d_{\text{Cu}\cdots\text{Cu}}$ 2.6485 Å).²⁹ This distance is even shorter than that found in [Cu₂I₂(THT)₄] (THT = tetrahydrothiophene) ($d_{\text{Cu}\cdots\text{Cu}}$ 2.675(2) Å).¹⁶

Increasing further the CuI amount to 4 equivalents led to the formation of the 2D **CP3** containing Cu₁(μ₂-I₂)(μ₄-I₁)Cu₂ SBUs (Figures 4 and S3). Each Cu₁-Cu₂ segment is

bridged by a μ_2 -type I2 atom with Cu1–I2 and Cu2–I2 distances of 2.5953(10) Å and 2.5791(10) Å, respectively. Three Cu1–Cu2 segments are capped by a μ_4 type I1 ligand with two coordination to the same Cu1–Cu2 segments and two to Cu1 and Cu2 atoms coming from two different segments. Quite similar motifs were encountered in the 1D ribbon obtained by reaction of 2-trimethylsilyl-1,3-dithiane with CuI.²² However, the connectivity between copper atoms differs in **CP3** with much shorter Cu1–Cu2 distance: 2.8584(13) Å vs 3.3975 Å but much longer Cu2–Cu2 and Cu1–Cu1 separations 3.361 Å vs 2.8203 Å for Cu1–Cu1 and 3.578 Å vs 3.362 Å for Cu2–Cu2. The experimental and simulated PXRD spectra of **CP1**, **CP2** and **CP3** are depicted in the Supporting Information as Fig. S11, S12 and S13, respectively..



Scheme 1. Synthesis of **CP1**, **CP2** and **CP3** employing various CuI-to-**L1** ratios.

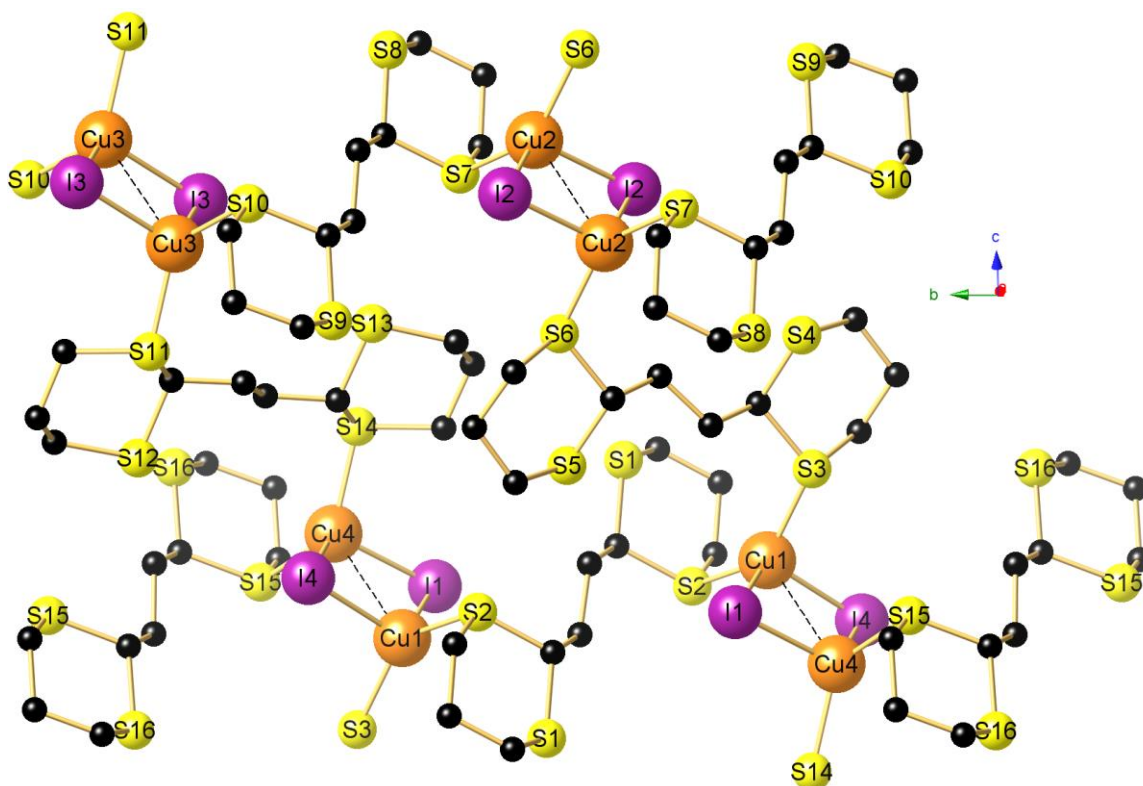


Figure 2. View down the a axis on a segment of the 2D layer of $[\{\text{Cu}(\mu_2\text{-I})_2\text{Cu}\}(\mu_2\text{-L1})_2]_n$ (**CP1**). Selected bond lengths (Å) at 100 K: Cu1–I1 2.6701(3), Cu1–I4⁴ 2.6761(3), Cu2–I2 2.6518(3), Cu2²–I2 2.6832(3), Cu3–I3 2.6440(3), Cu3³–I3 2.6936(3), Cu4–I4 2.6518(3), Cu4¹–I1 2.6761(3), Cu1–Cu4¹ 2.8820(4), Cu2–Cu2² 2.8399(5), Cu3–Cu3³ 2.9436(5), Cu1–S2 2.2880(5), Cu1–S3 2.2924(5), Cu2–S6 2.2829(5), Cu2–S7 2.2788(5), Cu3–S10 2.3139(5), Cu3–S11 2.3183(5), Cu4–S14 2.3157(5), Cu4–S15 2.3123(5), Symmetry transformations used to generate equivalent atoms: ¹ $+x, +y, 1+z$; ² $1-x, 2-y, 1-z$; ³ $1-x, 1-y, 1-z$; ⁴ $+x, +y, -1+z$.

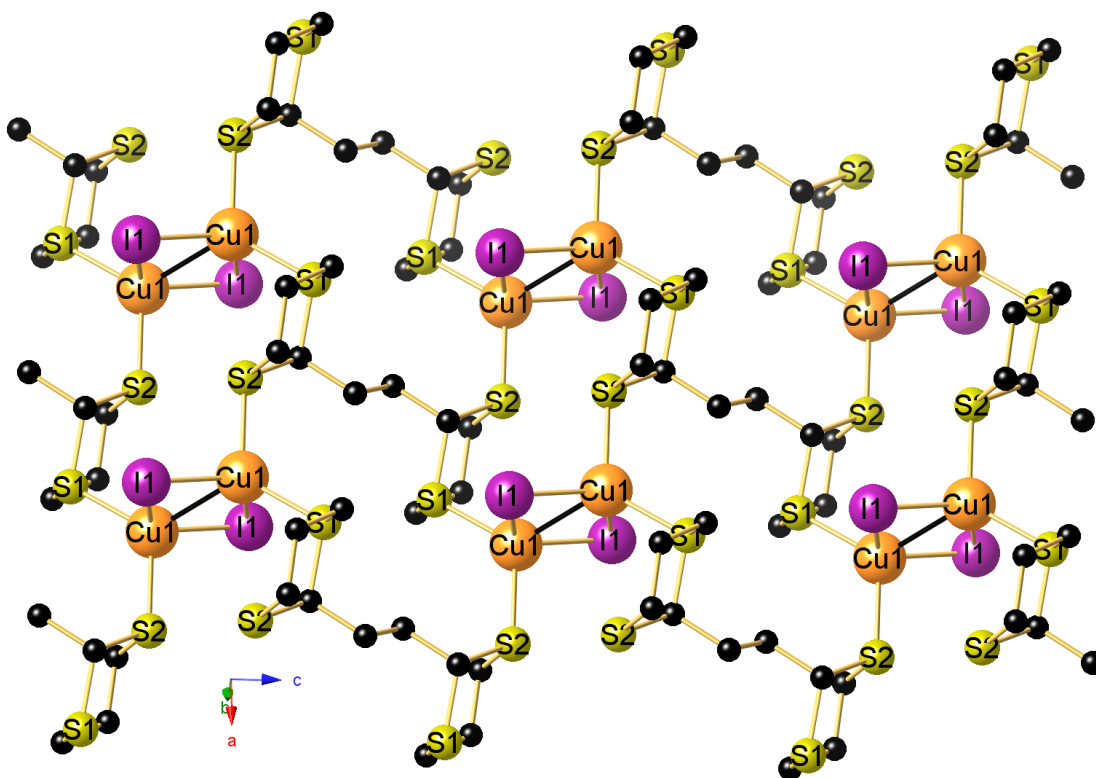


Figure 3. View down the b axis on a segment of the 2D layer of $[\{\text{Cu}(\mu_2\text{-I})_2\text{Cu}\}(\mu_4\text{-L})]_n$ (**CP2**). Selected bond lengths (Å) at 100 K: Cu–S1 2.3025(9), Cu–S2 2.3045(9), Cu–Cu# 2.6131(9), Cu–I 2.6414(5), Cu–I# 2.6690(5). Symmetry transformations used to generate equivalent atoms: $^1-x, 2-y, 1-y$; $^2-1+x, +y, +z$; $^31-x, 2-y, 2-z$.

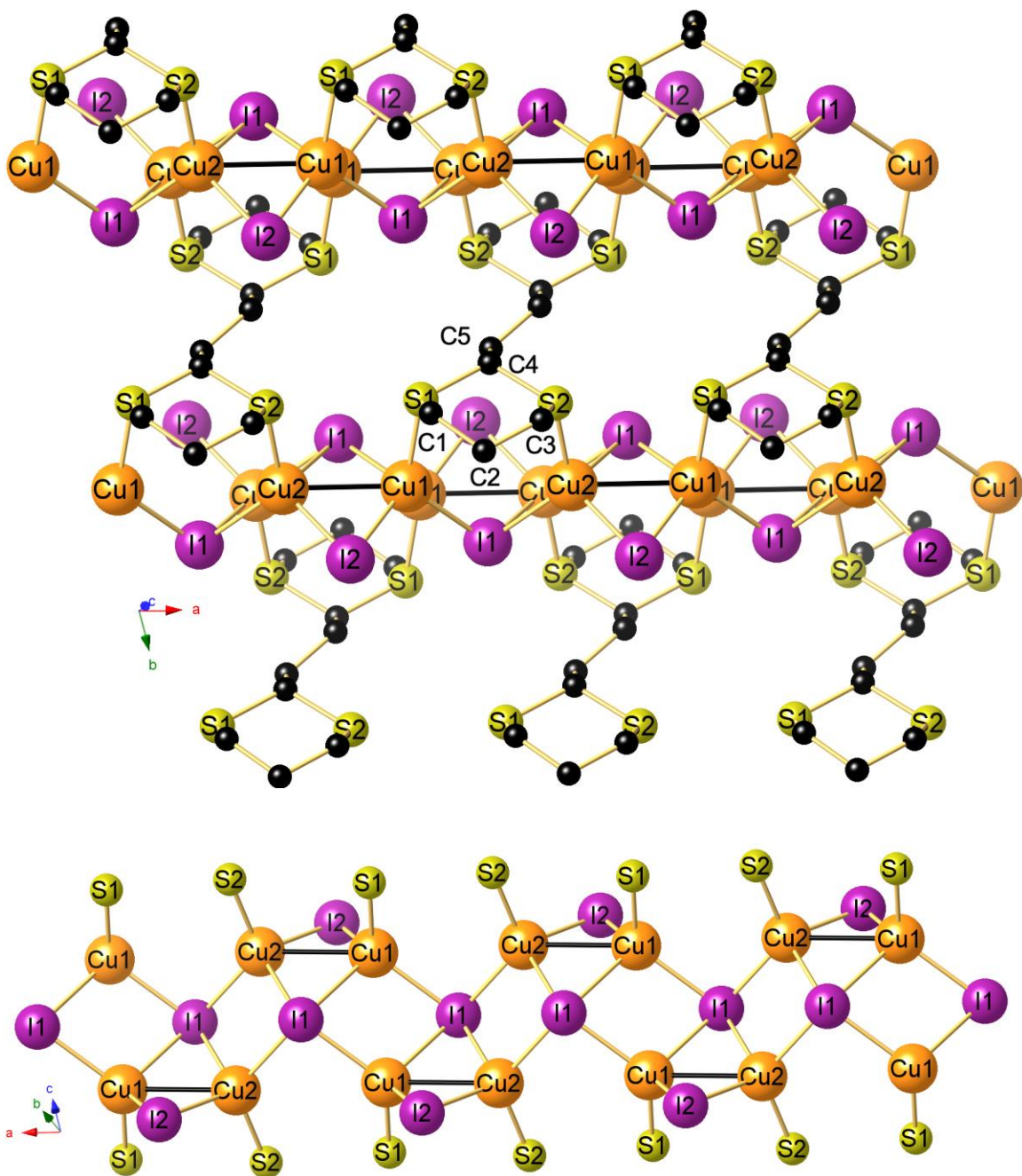


Figure 4. *Top* View down the *c* direction on a segment of the 2D layer of $[\{\text{Cu}(\mu_4\text{-I})(\mu_2\text{-I})\text{Cu}\}_2(\mu_4\text{-L1})]_n$ (CP3). Selected bond lengths (Å) at 100 K: I1–Cu1¹ 2.7914(10), I1–Cu1 2.6056(9), I1–Cu2 2.6043(11), I1–Cu2² 2.8749(12), I2–Cu1³ 2.5953(10), I2–Cu2 2.5791(10), Cu1–Cu2⁴ 2.8584(13), Cu1–S1 2.2713(17), Cu2–S2 2.2624(17) Symmetry transformations used to generate equivalent atoms: ¹ $-x, 1-y, 1-z$; ² $-x, 1-y, 1-z$; ³ $1+x, +y, +z$; ⁴ $-1+x, +y, +z$; ⁵ $-x, -y, 1-z$. *Bottom* view of the Cu1–Cu2 segments spanned by μ_2 -I and μ_4 -I atoms.

Reaction of **L1** with CuBr

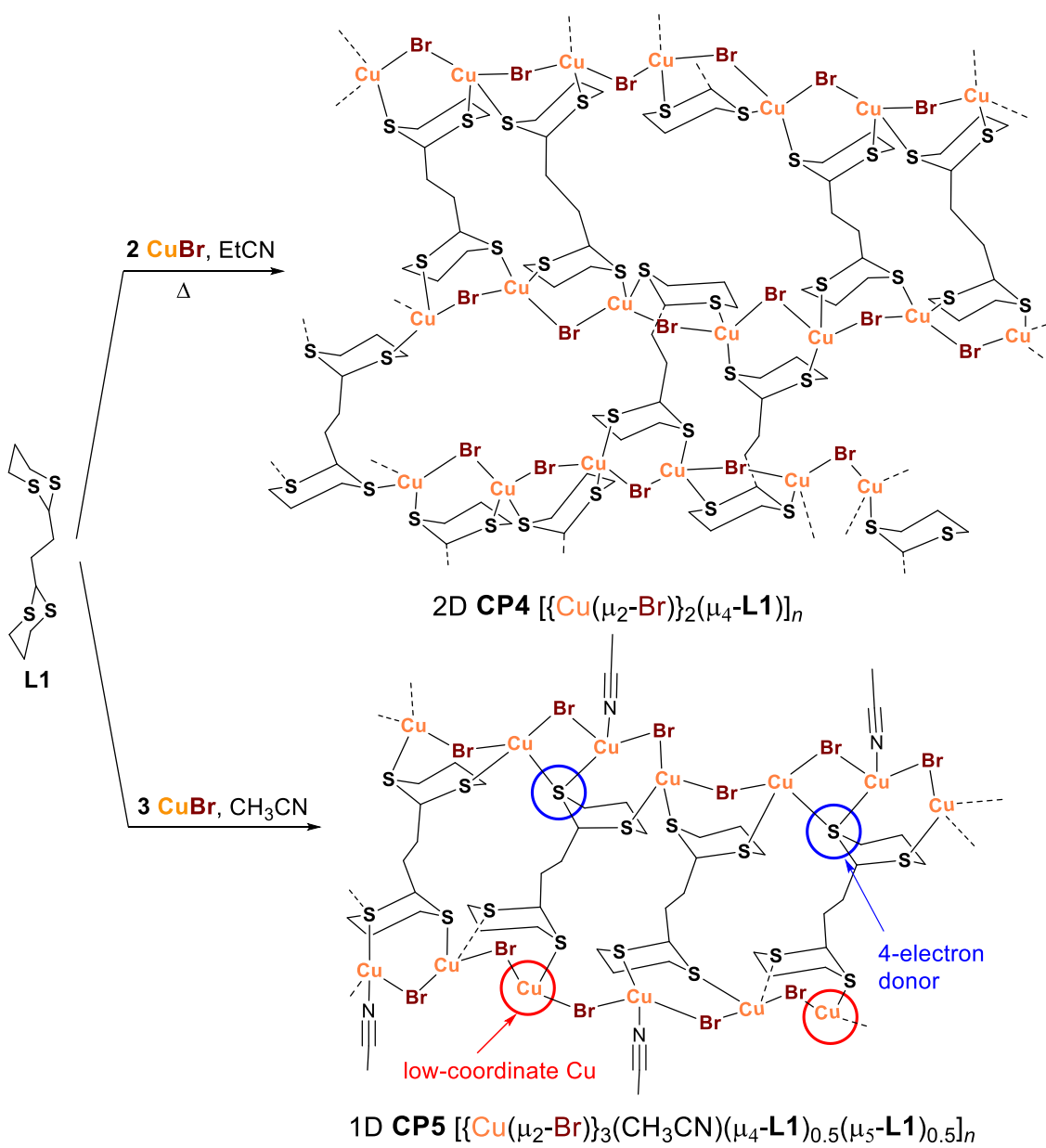
We recently reported the coordination of the 2-methyl-1,3-dithiane **L2** ligand toward CuBr in a 1:1 ratio. The crystal structure evidences the formation of the 1D CP $[\{\text{Cu}(\mu_2\text{-Br})_2\text{Cu}\}(\mu_2\text{-L2})_2]_n$ in which the SBUs are constituted of dinuclear $\text{Cu}(\mu_2\text{-Br})_2\text{Cu}$ rhomboids spanned by both sulphur atoms of **L2** with nonbonding $\text{Cu}\cdots\text{Cu}\#$ contacts of 3.176 Å.^{21, 22}

To compare the coordination properties of **L1** vs. **L2**, we reacted CuBr with **L1** employing a 2:1 metal-to-ligand ratio (Scheme 2). After addition of the ligand to a MeCN solution of CuBr, instantaneous precipitation of a large amount of a colourless product was noticed. However, since we failed to obtain X-ray-suitable single-crystals from hot MeCN, a part of the sample was dissolved in refluxing propionitrile in which crystals suitable for X-Ray analyses could be obtained. The resulting 2D material of composition $[\{\text{Cu}(\mu_2\text{-Br})_2\}(\mu_4\text{-L1})]_n$ **CP4** crystallized in the monoclinic space group $P2_1/c$ (Figures 5 and S4). The homogeneity of the sample was ascertained by recording the PXRD pattern (Fig. S12). Surprisingly, despite the similar reaction conditions for the preparation of $[\{\text{Cu}(\mu_2\text{-I})_2\text{Cu}\}(\mu_4\text{-L1})]_n$ (**CP2**), the 2D architecture of **CP4** shown in Figure 5 is strikingly different. The Cu atoms are not associated in the form of rhomboidal $\text{Cu}(\mu\text{-Br})_2\text{Cu}$ dimers but as isolated Cu atoms interconnected via a single μ_2 halide ligand with a Cu1-Cu2 distance of 3.681 Å, far above the sum of the van der Waals radii of two Cu atoms. The same structural arrangement was obtained in our group upon reaction of 1,3-dithiolane with CuBr in a 1:1 ratio leading to a 1D CP crystallizing, as **CP4**, in the $P2_1/c$ space group.²⁰ In **CP4**, the 2D-dimensionality is ensured through the use of the tetrathioether **L1** ligand. To our knowledge, these two CPs constitute the only examples encountered in thioether-assembled Cu(I) CPs.

Since both **L1** and the products of the reaction between **L1** and CuBr are poorly soluble in acetonitrile, we tried to grow crystals by slow diffusion of an acetonitrile solution of CuBr into a dichloromethane solution of **L1** in a 1:1 ratio. Well-shaped colourless crystals were obtained under these conditions. Surprisingly, a single-crystal diffraction analysis revealed the formation of a 1D material **CP5** having a composition $(\text{CuBr})_3(\text{L1})(\text{MeCN})$, *i.e.* a 3:1 metal-to-ligand ratio (Fig 6). We therefore repeated the reaction of **L1** with CuBr in acetonitrile using a 1:3 ratio (Scheme 2). Figure 7 shows the excellent concordance

between the experimental PXRD pattern recorded at room temperature for the obtained white precipitate and the calculated one issued from single crystal X-ray data recorded at 100 K. This confirms (i) the formation of the same product (**CP5**) and (ii) the absence of any phase transition in this 193 K range. Furthermore, elemental analyses also confirmed this 3:1 CuBr-to-**L1** composition. The IR spectrum of **CP5** also presents two weak peaks at 2309 and 2265 cm⁻¹ characteristic of the $\nu(\text{C}\equiv\text{N})$ vibration of coordinated acetonitrile (Figure S20).³⁰ As for **CP4**, the Cu atoms are interconnected through μ_2 -bromide ligands, but **CP5** contains (i) six crystallographically independent CuBr units, (ii) two differently ligating **L1** and (iii) two metal-bound acetonitrile molecules. Five of the copper(I) centers present CuBr₂S₂ (Cu3, Cu5 and Cu6) or CuBr₂NS (Cu1 and Cu4) classical tetrahedral coordination geometry. Surprisingly, Cu2 adopts a triangular CuBr₂S geometry with a sum of bond angles around Cu2(I) center ($\angle\text{Br3-Cu2-S3}$, $\angle\text{S3-Cu2-Br2}$ and $\angle\text{Br3-Cu2-Br2}$) equal to 359.97° and Cu2-S3, Cu2-Br3 and Cu2-Br2 bond lengths equal to 2.2173(11), 2.3649(7) and 2.3694(7) Å, respectively. The very loose Cu2...S6 contact of 3.045 Å cannot be considered as bonding.

Whereas a triangular geometry around a Cu(I) center has been encountered with thiolate and thion ligands,^{31, 32} to our knowledge, just only one other thioether example has been reported in the literature. In 2001, Schröder *et al* reacted CuCl with the tetradentate ligand 1,4,7,10-tetrathiacyclododecane ([12]aneS₄) yielding the mononuclear complex [CuCl([12]aneS₄)], for which the copper(I) centre is disordered over two positions in an approximate 7 : 1 ratio.⁹ In the minor component, the Cu atom adopts a distorted trigonal planar coordination geometry ($\Sigma(\text{angles}) = 359.5^\circ$) with two coordination to sulphur atoms [Cu-S 2.279(8), 2.320(8) Å] and one to a chloride ligand [Cu-Cl 2.266(7) Å]. Noteworthy in the unprecedented architecture of **CP5** is also the dissymmetric μ_4 -bonding mode of S1 atom with bridges as 4-electron donor both the Cu1 and Cu6 atoms [Cu1-S1 2.2730(11), Cu6-S1 2.7692(11) Å]. **CP5** extends to a 2D supramolecular layered framework through intermolecular C-H...Br interactions. (Fig. S5 and Table S8).



Scheme 2. Synthesis of CP4 and CP5.

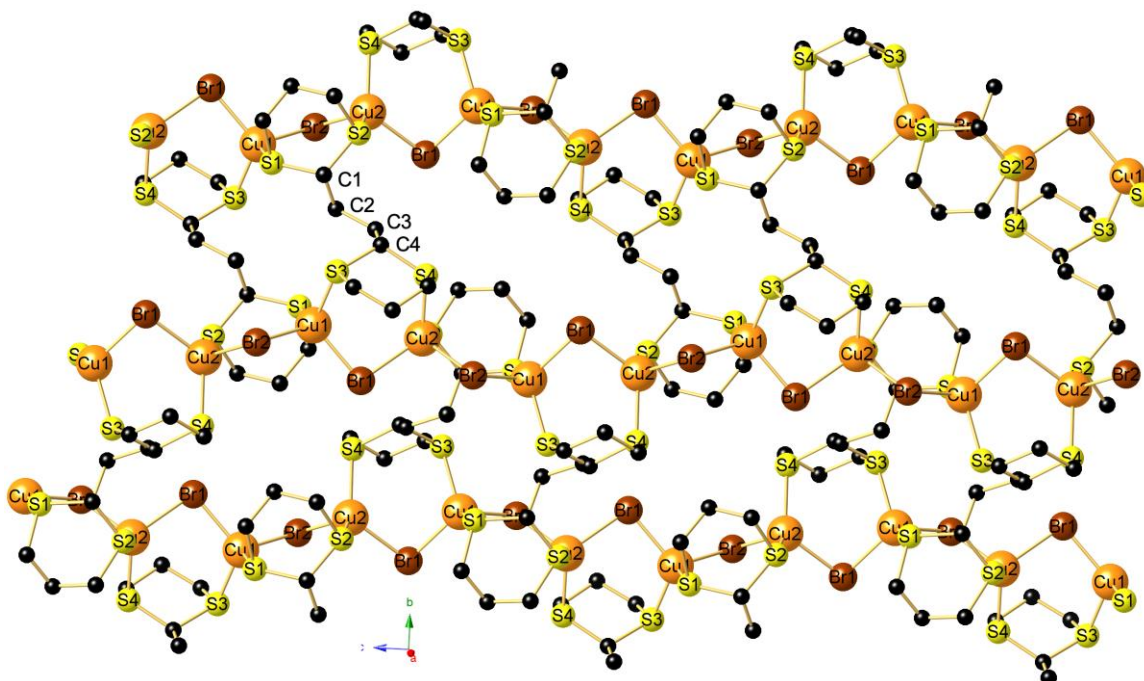


Figure 5. View down the *c* axis on a layer of the 2D network of $[\{\text{Cu}(\mu_2\text{-Br})\}_2(\mu_4\text{-L1})]_n$ (CP4). The H atoms are omitted for clarity. Selected bond lengths [Å] at 100 K: Cu1–S1 2.2857(7), Cu1–S3² 2.3220(7), Cu2–S2 2.2743(7), Cu2–S4³ 2.3046(7), Cu1–Br1 2.4525(5), Cu1–Br2 2.4887(5), Cu2¹–Br1 2.5229(5), Cu2–Br2 2.5022(5); Symmetry transformations used to generate equivalent atoms: ¹1+*x*, ½–*y*, ½+*z*; ²1–*x*, 1–*y*, 1–*z*; ³1–*x*, –1/2+*y*, 1/2–*z*; ⁴1–*x*, –1/2+*y*, 1/2–*z*.

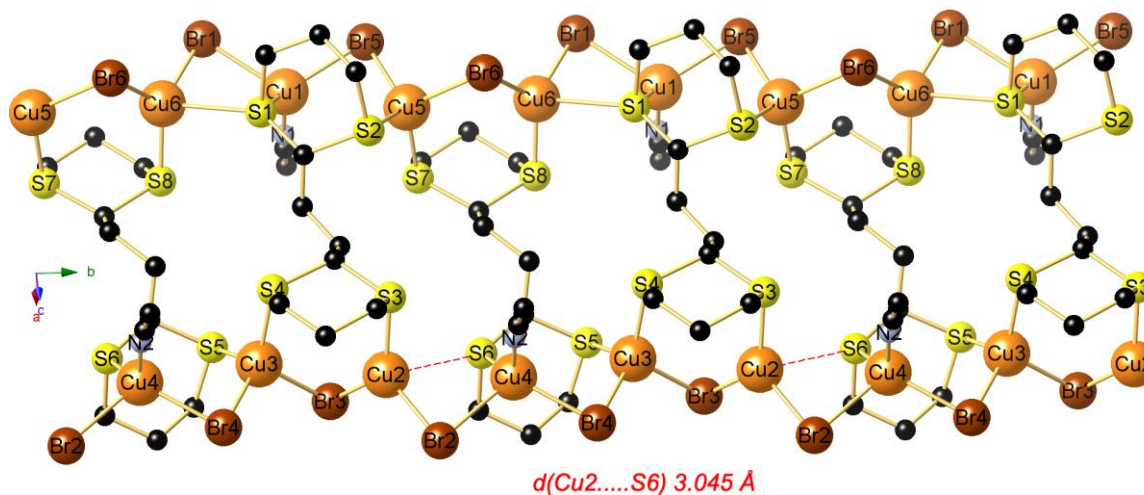


Figure 6. View of a segment of the 1D ribbon of $[\{\text{Cu}(\mu_2\text{-Br})\}_3(\text{MeCN})(\mu_4\text{-L1})_{0.5}(\mu_5\text{-L1})_{0.5}]_n$ (CP5) running along the *b* axis. The H atoms are omitted for clarity. Selected bond lengths [Å] at 100 K: Cu1–Br1 2.5911(7), Br1–Cu6 2.3911(7), Br2–Cu2 2.3694(7), Br2–Cu4¹ 2.5665(7), Br3–Cu2 2.3649(7), Br3–Cu3 2.5187(7), Br4–Cu3 2.4179(7), Br4–Cu4 2.4928(7), Br5–Cu1² 2.4852(7), Br5–Cu5 2.4270(6), Br6–Cu5 2.5198(6), Br6–Cu6 2.3610(7), Cu1–S1 2.2730(11), Cu1–N1 1.969(4), Cu2–S3 2.2173(11), Cu3–S4

2.2771(11), Cu3–S5 2.3222(11), Cu4–S6 2.2772(12), Cu4–N2 1.984(4), Cu5–S2² 2.3362(11), Cu5–S7 2.2716(11), Cu6–S1 2.7692(11), Cu6–S8 2.2299(12), Cu2–S3 2.2173(11), Cu3–S4 2.2771(11), Cu3–S5 2.3222(11), Cu4–S6 2.2772(12), Cu4–N2 1.984(4), Cu5–S2² 2.3362(11), Cu5–S7 2.2716(11), Cu6–S1 2.7692(11), Cu6–S8 2.2299(12); Symmetry transformations used to generate equivalent atoms: ¹+x,-1+y,+z; ²+x,1+y,+z.

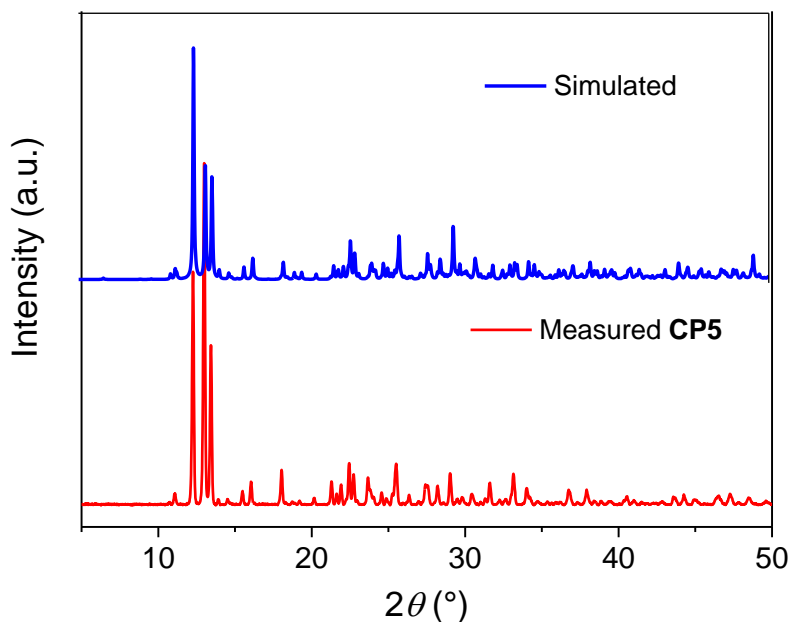
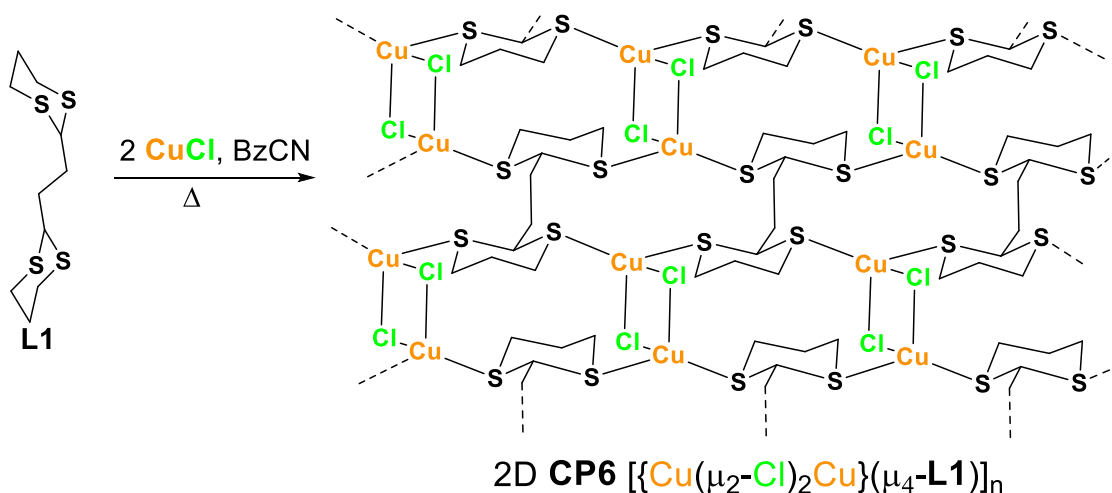


Figure 7. Comparison of the experimental PXRD pattern of **CP5** with the simulated one.

*Reaction of **L1** with CuCl*

The coordination aptitude of **L1** towards CuCl was also compared to that of **L2**. For memory, we have shown that, when reacting **L2** with CuCl in a 1:1 ratio, the 1D CP [$\{\text{Cu}(\mu_2\text{-Cl})_2\text{Cu}\}(\mu_2\text{-L2})_2$]_n was obtained, in which the SBUs are constituted of dinuclear Cu($\mu_2\text{-Cl})_2\text{Cu}$ rhomboids.²²

Fast and almost quantitative precipitation of a colourless product occurred also upon mixing a MeCN solution of **L1** with two equivalents of CuCl (Scheme 3). Since attempts to grow X-ray suitable crystals from hot MeCN failed due to its poor solubility, a sample was dissolved in hot benzyl cyanide.



Scheme 3. Synthesis of **CP6**.

Now, small needle-shaped single crystals could be grown, crystallizing in the monoclinic space group $C2/m$. In line with the elemental analysis, an X-ray diffraction analysis confirmed a composition of two CuCl units per **L1** molecule. The crystal structure of $[\{\text{Cu}(\mu_2\text{-Cl})_2\text{Cu}\}(\mu_4\text{-L1})]_n$ (**CP6**) shown in Figures 8 and S6 reveals formation of a two-dimensional network, in which centrosymmetric $\{\text{Cu}(\mu_2\text{-Cl})_2\text{Cu}\}$ SBUs are interconnected through bridging **L1** molecules, in which all 4 S-donors are involved in the bonding, reminiscent to the architecture of $\{\text{Cu}(\mu_2\text{-I})_2\text{Cu}\}(\mu_4\text{-L1})]_n$ (**CP2**). Like in the latter, all 4 atoms of the $\{\text{Cu}(\mu_2\text{-X})_2\text{Cu}\}$ units lie in the same plane. However, whereas in **CP2** the Cu \cdots Cu contacts are unusually short, those of **CP6** are now extremely elongated and lie now at the far side (2.6131(9) vs. 3.147 Å). Among the rare examples of 2D networks incorporating $\{\text{S}_2\text{Cu}(\mu_2\text{-Cl})_2\text{CuS}_2\}$ rhomboids are $[\{\text{Cu}(\mu_2\text{-Cl})_2\text{Cu}\}\{\mu\text{-BzS}(\text{CH}_2)_6\text{SBz}\}_2]_n$ ($d\text{Cu}\cdots\text{Cu}$ 2.9570(14) Å) and $[\{\text{Cu}(\mu_2\text{-Cl})_2\text{Cu}\}\{\mu\text{-BzS}(\text{CH}_2)_7\text{SBz}\}_2]_n$ ($d\text{Cu}\cdots\text{Cu}$ 2.6939(4) Å).²⁸ The comparison of these three CuCl-based 2D compounds demonstrates that also in $\{\text{Cu}(\mu_2\text{-Cl})_2\text{Cu}\}$ rhomboids an extreme flexibility of the Cu \cdots Cu contacts may occur ranging from bonding to clearly non-bonding. Note that as mentioned above, in the reaction of CuCl with 2-methyldithiane **L2**, a 1D ribbon $[\{\text{Cu}(\mu_2\text{-Cl})_2\text{Cu}\}(\mu_2\text{-L2})_2]_n$ was generated, featuring somewhat shorter Cu \cdots Cu contacts with respect to those of **CP6** (3.0517(8) vs. 3.147 Å). The Cu–S bond length of **CP6** matches with that of $[\{\text{Cu}(\mu_2\text{-Cl})_2\text{Cu}\}(\mu_2\text{-L2})_2]_n$ (2.2924(8) vs. 2.3060(4) Å).²² The experimental and simulated PXRD patterns of **CP6** are depicted in the Supporting Information as Fig. S15.

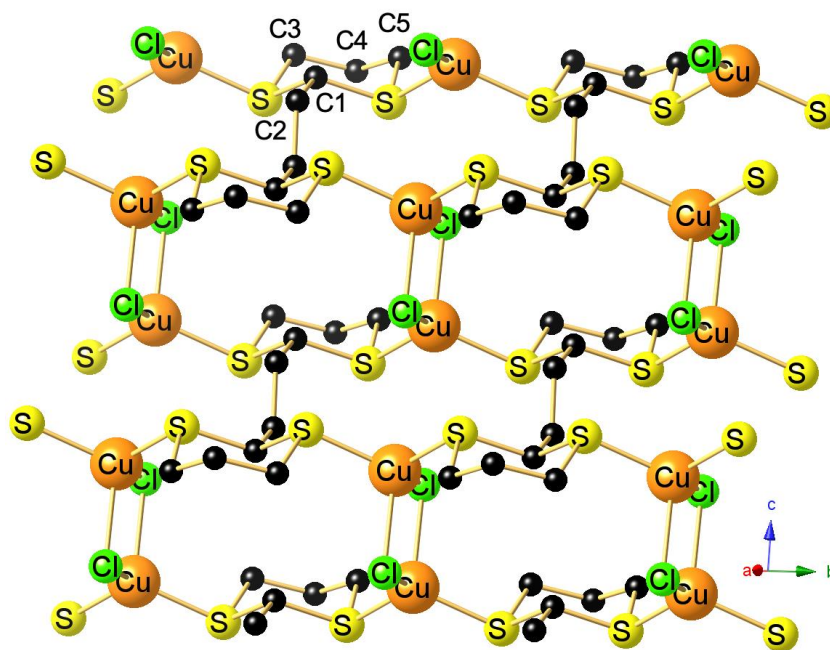


Figure 8. View down the *a* axis on a segment of the 2D layer of $[\{\text{Cu}(\mu_2\text{-Cl})_2\text{Cu}\}(\mu_4\text{-L1})]_n$ (**CP6**). The H atoms are omitted for clarity. Selected bond lengths (Å) and angles (°) at 100 K: Cu–S 2.2924(8), Cu···Cu# 3.147, Cu–Cl 2.2961(11), Cu–Cl# 2.4549(12); S–Cu–S# 109.01(4), S–Cu–Cl 118.74(2), S–Cu–Cl# 105.28(3), Cl–Cu–Cl# 97.110(14), Cu–Cl–Cu# 82.89(4). Symmetry transformations used to generate equivalent atoms: $^11-x, 2-y, 2-z$; $^2+x, 2-y, +z$; $^31-x, 1-y, 1-z$.

Reaction of **L1** and **L2** with HgI_2

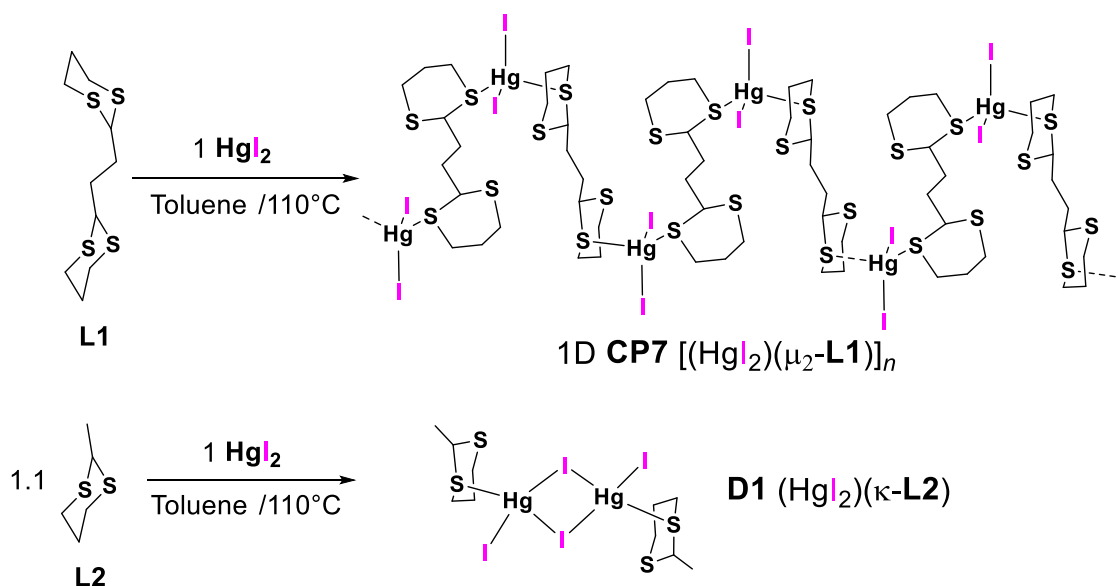
Another soft metal ion having a high affinity to organosulfur ligands is the closed-shell d^{10} Hg(II) ion. Selected examples of molecular complexes and CPs ligated with dialkylsulfides and acyclic dithioether are $\text{CH}_3\text{SCH}_2\text{CH}_3 \cdot \text{HgCl}_2$,³³ $[\text{HgCl}_2(\text{CH}_3\text{SPh})]_n$,³⁴ $[(\text{EtS}(\text{CH}_2)_2\text{SEt})\text{HgBr}(\mu\text{-Br})\text{Hg}(\text{Br})(\mu\text{-Br})_2\text{Hg}(\text{Br})(\mu\text{-Br})\text{BrHg}(\text{EtS}(\text{CH}_2)_2\text{SEt})] \cdot 2\text{HgBr}_2$,³⁵ $[\{\text{EtS}(\text{CH}_2)_2\text{SEt}\}\text{Hg}_2\text{Br}_4]_n$,³⁶ $[\{\text{BzS}(\text{CH}_2)_4\text{SBz}\}\text{Hg}_2\text{Br}_4]_n$,³⁷ $[\{\text{BzS}(\text{CH}_2)_4\text{SBz}\}\text{HgBr}_2]_n$,³⁸ $[\{\text{PhS}(\text{CH}_2)_2\text{SPh}\}\text{Hg}_2\text{Br}_4]_n$,³⁹ and $\text{HgX}_2 \text{RSCH}_2\text{C}_6\text{H}_4\text{CH}_2\text{SR}$.⁴⁰ Our group has, in the past, investigated the coordination of the dithioether 1,4-bis(phenylthio)butane with HgCl_2 and HgBr_2 producing the isostructural 2D CPs $[\{\text{PhS}(\text{CH}_2)_4\text{SPh}\}\text{Hg}_2\text{X}_4]_n$ and that of $(\text{PhSCH}_2)_2\text{SiPh}_2$ leading to the discrete molecular complex $[\text{HgBr}_2\{(\text{PhSCH}_2)_2\text{SiPh}_2\}]$.^{41, 42}

We were intrigued whether **L1** could be used as assembling ligand to construct original coordination network as observed with CuX salts. This is *a priori* not a evident task, since

several papers report on the use of Hg(II) salts as Lewis acids to cleave cyclic thioacetals such as dithiolanes and dithianes, converting them to aldehydes or ketones.⁴³⁻⁴⁵ For example, a protocol allowing an efficient and fast deprotection of cyclic thioacetals by Hg(NO₃)₂ even in the solid state has been described.⁴⁶

On the other hand, an IR spectroscopic investigation dating from the sixties indicated formations of tetrahedral adducts HgX₂S₂ through equatorial donation of a sulphur lone-pair of 1,3-dithiane. According to this study, the mercury-sulphur bond varies in strength in the order Cl > Br > I.⁴⁷ An adduct formation between Hg(OAc)₂ and 1,3-dithiane in solution was also evidenced by ¹⁹⁹Hg NMR spectroscopy.⁴⁸ An ESI-mass spectroscopy investigation indicated formation of a stable associate between HgCl₂ and 1,1'-bis(1,3-dithiane-2-yl)ferrocene.⁴⁹ Even the possibility to use 1,3-dithiane as assembling ligand for the construction of a CP has been demonstrated in the seventies by the crystallographic characterization of 1D-polymeric 1,3-dithiane-dimercury(I) dinitrate.^{50, 51}

We first treated **L1** with two equivalents of HgI₂ in refluxing toluene. However, even after a reaction time of several hours, unreacted red α-HgI₂ co-crystalized along with the pale-yellow product [(HgI₂)(μ₂-**L1**)]_n (**CP7**). To circumvent this co-crystallization, addition of a further equivalent of **L1** was required to complete the reaction, allowing to isolate now pure **CP7** in over 85% yield (Scheme 4).



Scheme 4. Synthesis of **CP7** and **D1**.

A crystal structure determination (Fig. 9) of this air-stable material confirmed the 1:1 metal-to-ligand composition. This material forms a meander-like 1D ribbon, in which HgI_2 units are exclusively ligated through the S1 and S3 atoms of the centrosymmetric **L1** molecules. The S2 and S4 atoms are not involved in any Hg–S bonding. The mean Hg–S bond length of 2.6574(8) Å matches well with those reported for 1D CP $[\text{HgI}_2\{\mu_2\text{-1,4-bis(methylsulfanyl)methylbenzene}\}]_n$ (2.6431(13) and 2.6619(13) Å).⁴⁰ Far longer Hg–S bond lengths are found for the dinuclear complex $[(\text{HgI}_2)_2(\mu_2\text{-(1,2,4,5-tetrakis(cyclohexylsulfanyl)methyl)benzene})]$ (2.749(3) and 2.787(3) Å) and 1D-polymeric $[\text{HgI}_2(\mu\text{-1,4,8,11-tetrathiacyclotetradecane})]_n$ (2.752 (3) Å).^{52, 53} The two Hg–I bond lengths are slightly different, their mean distance of 2.7077(2) Å is similar to that of $[\text{HgI}_2(\mu_2\text{-1,4-bis((methylsulfanyl)methyl)benzene})]_n$ (2.7241(4) Å). For the latter two compounds, the mean Hg–I bond lengths are shorter and lie between 2.661(2) and 2.658(1) Å. The coordination sphere around the mercury atom is somewhat distorted from regular tetrahedral; the bond angles range 102.866–121.843°. The I1–Hg–I2 angle of 121.843° is more acute than for the other three compounds, which are 124.98(2), 145.87(3), and 136.31(6)°, respectively. The experimental and simulated PXRD patterns of **CP7** are depicted in the Supporting Information as Fig. S16.

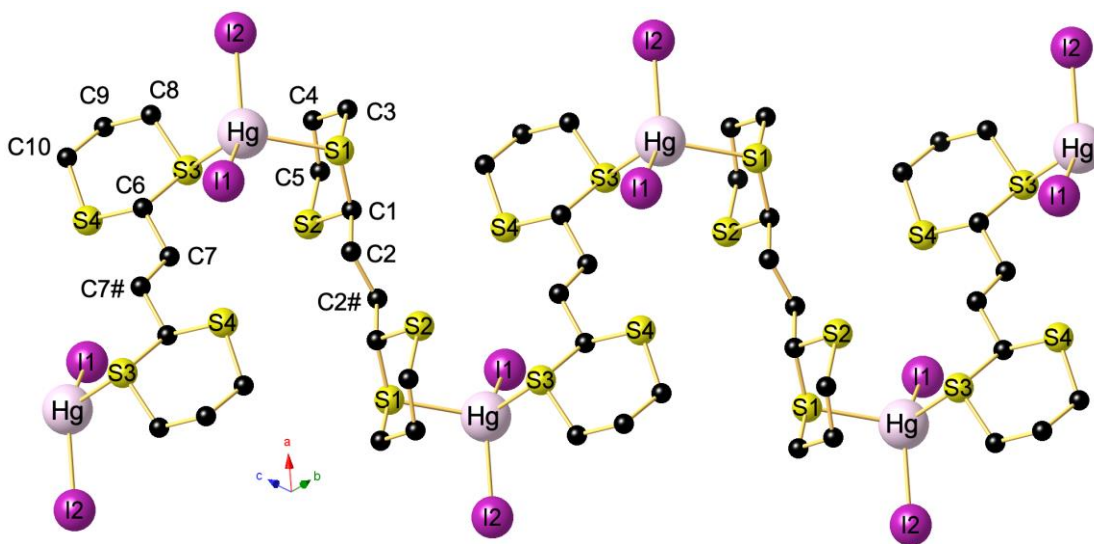


Figure 9. View of a segment of the 1D chain of $[(\text{HgI}_2)(\mu_2\text{-L1})]_n$ (**CP7**). The H atoms are omitted for clarity. Selected bond lengths (Å) and angles (°) at 100 K: Hg–S1 2.6712(8), Hg–S3 2.6436(7), Hg–I1 2.6950(2), Hg–I2 2.7203(2); S1–Hg–S3 110.53(2), S1–Hg–I1 105.027(17), S1–Hg–I2 102.866(17), S3–Hg–I1 110.603(17), S3–Hg–I2 105.53(2), I1–Hg–I2 121.843(8), Symmetry transformations used to generate equivalent atoms: ¹2-*x*, -*y*, 2-*z*; ²2-*x*, 1-*y*, 1-*z*.

A survey of the CSD database (version 5.41 – March 2020 update) reveals that despite an indexation of over 135 entries for $\text{HgX}_2 \cdot \text{thioether}$ compounds, most of these examples are dominated by HgCl_2 and HgBr_2 adducts. The few examples of HgI_2 adducts are essentially thiamacrocyclic complexes such as 1D $[\text{HgI}_2(\mu\text{-}1,4,8,11\text{-tetrathiacyclotetradecane})]_n$ or the molecular complex $[\text{HgI}_2(2,5\text{-dioxo-}8,11\text{-dithia-}1,6(1,2)\text{-dibenzenacyclododecaphane-}S,S')]$.^{52, 53} Among the few acyclic HgI_2 adducts are the above mentioned CP $[\text{HgI}_2\{\mu\text{-}1,4\text{-bis(methylsulfanyl)methyl)benzene}\}]_n$ and dinuclear $[(\text{HgI}_2)_2(\mu\text{-}(1,2,4,5\text{-tetrakis(cyclohexylsulfanyl)methyl)benzene})]$.^{40, 53} This paucity of structurally characterized HgI_2 adducts and the fact that HgI_2 does not form a 2:1 material with **L1**, intrigued us to conduct the analogous reaction with 2-methyl-1,3-dithiane **L2**. Although sterically less crowded than **L1**, we failed to convert entirely HgI_2 to a thioether complex even in hot toluene, using a 1:1 **L2**-to-Hg ratio. The co-crystallization of HgI_2 could only be suppressed by adding a slight excess of **L2** to a toluene suspension of HgI_2 (Scheme 4). After this modification, the thioether adduct **D1** was straightforwardly obtained upon heating in toluene during 2h. After allowing to reach ambient temperature, a product of composition $[(\text{HgI}_2)(\text{L2})]$ crystallized in form of large yellow blocks. Surprisingly, instead of an anticipated polymeric network, an X-ray diffraction study revealed formation of a discrete dinuclear complex $[\{\text{IHg}(\mu\text{-I})_2\text{HgI}\}(\kappa^1\text{-L2})_2]$ **D1** (Fig. 10). In this molecular compound, which, from a topological point of view, is considered formally a 0D, each Hg(II) atom bears one terminal I2 ligand, the second I1 ligand is $\mu\text{-}$ bridging assuring the connectivity with the neighbored Hg atoms. The intermetallic separation of 4.099 Å is far too loose to be considered as bonding. The distorted tetrahedral coordination around each mercury atom is completed by a dative bond with the S1 atom of the **L2** ligand, where the S2 atom does not participate in bonding. To the best of our knowledge, there is just one other crystallographically molecular complex featuring a $\text{S(I)Hg}(\mu\text{-I})_2\text{Hg(I)S}$ scaffold, namely $[(\text{NO}_2\text{S}_2)\text{S(I)Hg}(\mu\text{-I})_2\text{Hg(I)(NO}_2\text{S}_2)]$ ligated by the 18-membered thiaoxamacrocyclic bis(16-(4-(4-nitrophenylazo)phenyl)-2,5-dioxo-13,19-dithia-16-azatricyclo(19.4.0.06,11)pentacosa-1(21),6,8,10,22,24-hexaene) (CSD refcode PEGXU).^{54, 55} The metric parameters of the latter complex are quite similar with those of **D1**. In both compounds, the three Hg-I bond distances are quite different, the shortest being

the terminal one (2.6920(6) vs. 2.6610(3) Å), the bond lengths of the dissymmetrically bridging μ_2 -iodo ligand are 2.7080(6) vs. 2.7252(3) and 3.1541(7) vs. 3.2078(3) Å, respectively. Also, the Hg–S bond lengths of the two compounds match well (2.5983(18) vs. 2.5962(9) Å).

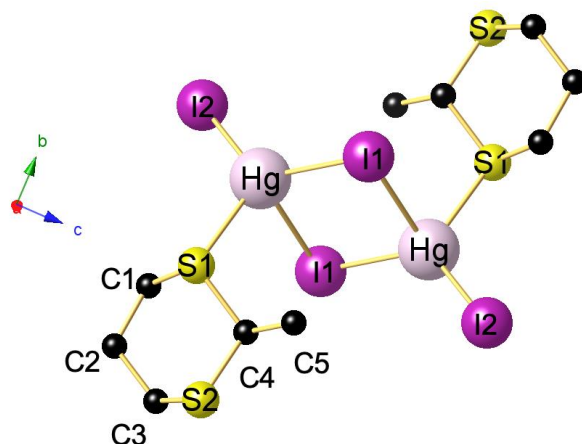
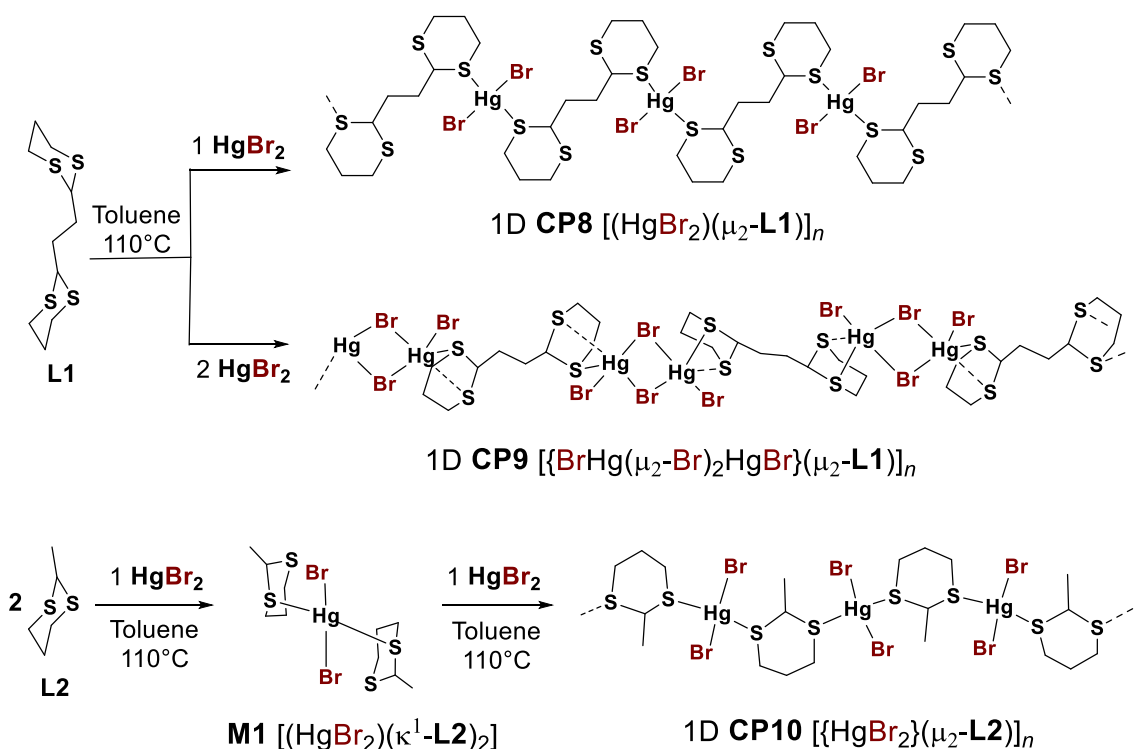


Figure 10. View of dinuclear complex $[\{ \text{IHg}(\mu_2\text{-I})_2\text{HgI} \}(\kappa^1\text{-L2})_2]$ (**D1**). The H atoms are omitted for clarity. Selected bond lengths (Å) and angles (°) at 100 K: Hg–S1 2.5962(9), Hg–I1 2.7252(3), Hg–I2 2.6610(3), Hg–I1# 3.2078(3); S1–Hg–I1 114.35(2), S1–Hg–I2 116.58(2), S1–Hg–I1# 91.07(2), I1–Hg–I2 127.203(11), I1–Hg–I1# 92.996(10). Symmetry transformation used to generate equivalent atoms: $^11-x, 1-y, 1-z$.

*Reactions of **L1** and **L2** with HgBr_2*

To investigate the effect of the nature of the halide on the architecture, **L1** was also mixed with one equivalent of HgBr_2 and heated in hot toluene for 3h. After allowing to reach ambient temperature, colourless needle-shaped crystals were formed and isolated in 68% yield (Scheme 5). Elemental analysis confirmed a 1:1 composition $[(\text{HgBr}_2)(\text{L1})]$ as for **CP7**.



Scheme 5. Synthesis of **CP8**, **CP9**, **M1** and **CP10**.

However, crystallographic analysis indicated that instead of the triclinic space group *P-1* encountered for **CP7** this material had crystallized in the orthorhombic space group *Pna2₁* (Table S5). Indeed, an X-ray diffraction study revealed that in the 1D polymeric ribbon of $[(\text{HgBr}_2)(\mu_2\text{-L1})]_n$ (**CP8**) shown in Figure 11, the meander-like conformation of **CP7** is no longer present and a description as linear is more appropriate. Each tetrahedrally coordinated Hg center is ligated by two terminal bromide ligands and the S1 and S4 donor sites of **L1**. The mean Hg–S bond length of **CP8** is slightly shorter than that of its iodo-analogue **CP7** (2.6362(16) vs. of 2.6574(16) Å). A somewhat reminiscent single-chain structure has been reported for $[\{\text{BzS}(\text{CH}_2)_4\text{SBz}\}\text{HgBr}_2]_n$, in which adjacent HgBr_2 units (Hg–Br 2.5823(8) and 2.5165(8) Å) are linked by the bridging dithioether ligand.³⁸ The packing of the parallel running ribbons of **CP8** is shown in the ESI as Figure S7 and the experimental and simulated PXRD patterns of **CP8** are depicted in the Supporting Information as Fig. S17.

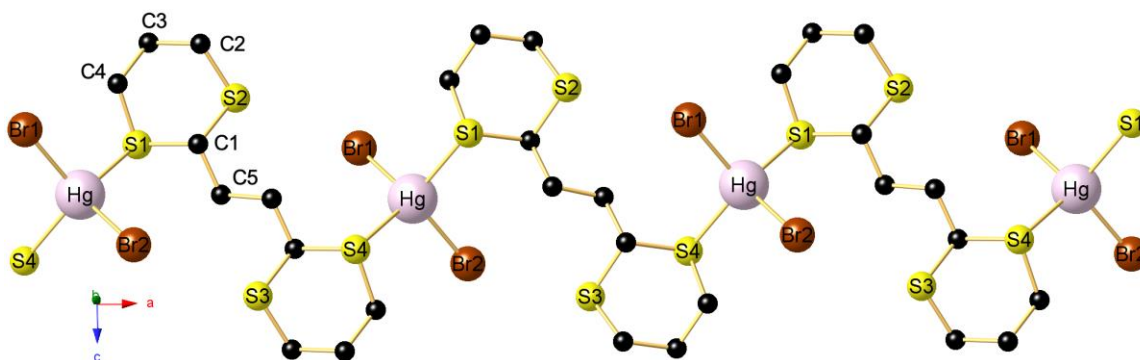


Figure 11. View of a segment of the 1D chain of $[(\text{HgBr}_2)(\mu_2\text{-L1})]_n$ (**CP8**). The H atoms are omitted for clarity. Selected bond lengths (\AA) and angles ($^\circ$) at 100 K: Hg–S1 2.6098(16), Hg–S4 2.6625(16), Hg–Br1 2.5841(11), Hg–Br2 2.5810(11); S1–Hg–S4 116.69(4), S1–Hg–Br1 103.77(4), S1–Hg–Br2 108.63(4), S4–Hg–Br1 108.42(4), S4–Hg–Br2 103.80(4), Br1–Hg–Br2 115.716(18), Symmetry transformations used to generate equivalent atoms: $^1\text{-}1/2+x, 1/2-y, +z$; $^2\text{-}1/2+x, 1/2-y, +z$.

The same simple tetrahedral HgBr_2S_2 motif was obtained when reacting HgBr_2 with an excess of **L2** in hot toluene. Upon cooling, fine colourless needles of the mononuclear complex $[\text{HgBr}_2(\kappa^1\text{-L2})_2]$ (**M1**) crystallizing in the orthorhombic space groups $P2_12_12$ (Table S7) were formed in 86% yield (Scheme 5). The molecular structure of **M1** is shown in Figure 12 and consists of a bent HgBr_2 unit coordinated by two κ^1 -bound 2-methyldithiane ligands. The Hg–S bond length is slightly shorter than the mean distance found in **CP8** (2.6188(17) vs. 2.6362(16) \AA). In contrast to $[\text{HgBr}_2\{(\text{PhSCH}_2)_2\text{SiPh}_2\}]$,⁴¹ in which the HgBr_2 angle is close to linearity, the angle Br–Hg–Br of **M1** is strongly bent (160.39(4) vs. 115.96(3) $^\circ$). The only other crystallographically characterized molecular HgBr_2 complex ligated by a non-macrocyclic thioether ligand is $[\text{HgBr}_2(N\text{-Benzoyl-1,3-thiazolidine})_2]$ (CSD refcode DICMEI) which features a more distorted tetrahedral geometry than **M1** with Br–Hg–Br and S–Hg–S angles of 124.4(9) and 83.9(2) $^\circ$, respectively.⁵⁶ With the objective to prepare a dinuclear compound $[\{\text{BrIHg}(\mu_2\text{-Br})_2\text{HgBr}\}(\kappa^1\text{-L2})_2]$ comparable to **D1**, **M1** was reacted with an second equivalent of HgBr_2 in hot toluene according to Scheme 5. To our surprise, a single-crystal diffraction study revealed formation of a colourless 1D polymeric material $[\text{HgBr}_2(\mu_2\text{-L2})]_n$ (**CP10**). The crystal structure of **CP10** is shown in Figures 13 and S9 and presents a highly symmetric 1D chain with crystallography identical S atoms. The most relevant bond

distances and angles are given in the caption of Figure 13 and deserve no special comment. Noteworthy is the occurrence of some weak intermolecular $\text{H}\cdots\text{Br}$ bonding between the parallel running 1D chains of **CP10** generating a 3D supramolecular network (Fig. S9 and Table S9).

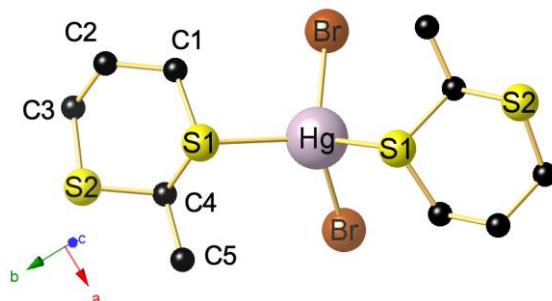


Figure 12. View of the molecular structure of $[(\text{HgBr}_2)(\kappa^1\text{-L2})]$ (**M1**). The H atoms are omitted for clarity. Selected bond lengths (Å) and angles (°) at 100 K: Hg–S1 2.6188(7), Hg–Br 2.5913(7); S1–Hg–S1¹ 118.90(7), S1–Hg–Br 109.06(4), Br–Hg–Br¹ 115.96(3), Symmetry transformation used to generate equivalent atoms: ¹1-*x*, 1-*y*, +*z*.

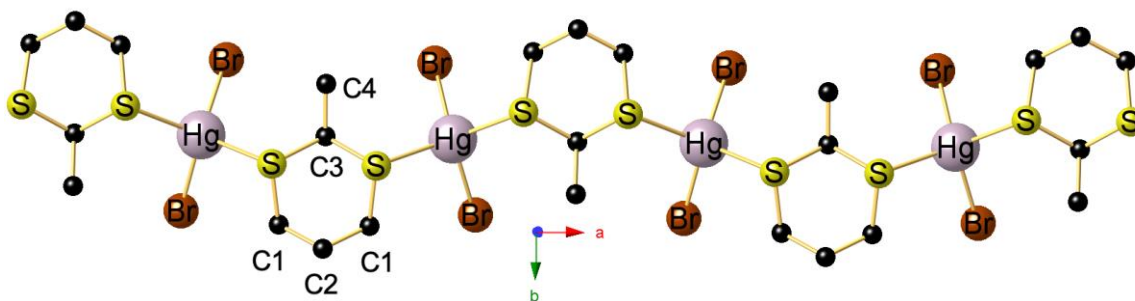


Figure 13. View of a segment of the 1D chain of $[(\text{HgBr}_2)(\mu_2\text{-L2})]_n$ (**CP10**) running along the *a* axis. The H atoms are omitted for clarity. Selected bond lengths (Å) and angles (°) at 100 K: Hg–S 2.6486(10), Hg–Br 2.5553(5); S1–Hg–S1¹ 113.21 (5), S–Hg–Br 102.46(4), S–Hg–Br¹ 109.81(2), Br–Hg–Br¹ 115.576(3), Symmetry transformation used to generate equivalent atoms: ¹1-*x*, 1-*y*, +*z*; ²1/2-*x*, +*y*, +*z*.

We next treated **L1** with two equivalents of HgBr_2 in refluxing toluene. In this case, isolation of the pure reaction product was not hampered by co-crystallization of unreacted HgBr_2 . Elemental analysis of the needle-shaped colourless material, which has been isolated in 76% yield, supported a 2:1 HgBr_2 -to-**L1** ratio HgBr_2 (Scheme 5). An X-ray diffraction study of the product $[\{\text{BrHg}(\mu_2\text{-Br})_2\text{HgBr}\}(\mu_2\text{-L1})]$ (**CP9**), crystallizing in the monoclinic space group $C2/c$ corroborates this composition. The crystal structure shown

in Fig. 14 reveals the formation of 1D ribbons, in which dinuclear $\text{BrHg}(\mu_2\text{-Br})_2\text{HgBr}$ units are interconnected through bridging centrosymmetric **L1** molecules. In contrast to the meander-type architecture of **CP7**, that of **CP9** can be described as stretched linear. The alignment of the parallel running ribbons in the packing is shown in Fig. S8. Within the dinuclear Hg_2Br_4 SBUs, the two crystallographically identical Hg atoms are solely connected through two bridging bromo ligands, the loose separation of 4.091 Å excludes any intermetallic interaction. Overall, the motif is quite reminiscent to that of **D1**. Among the 30 entries for $\text{HgBr}_2 \cdot$ thioether adducts, there are two examples featuring a similar unit, namely 1D CP $[\text{Hg}_2\text{Br}_4\{\text{BzS}(\text{CH}_2)_4\text{SBz}\}]_n$ ($d\text{Hg}\cdots\text{Hg}$ 3.884 Å) and the molecular complex $[\text{Hg}_2\text{Br}_4(\text{phenothiazine-S})]$ ($d\text{Hg}\cdots\text{Hg}$ 4.001 Å).^{37, 57}

Each Hg atom is tetrahedrally coordinated by one terminal Br2 atom, two μ_2 -type Br1 atoms and a datively bound S1 atom. The mean Hg–S bond length is somewhat shorter than that of **CP8** (2.5456(8) vs. 2.5825(11) Å). There is furthermore a very loose contact of 3.149 Å between the S2 atom and the Hg center, represented by the dashed lines in Fig. 14. Taking in account this incipient pentacoordination, the geometry may be alternatively considered as square pyramidal with Br2 occupying the apical position.

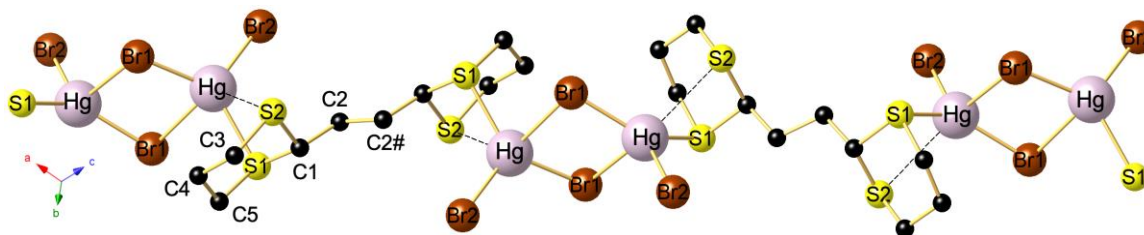
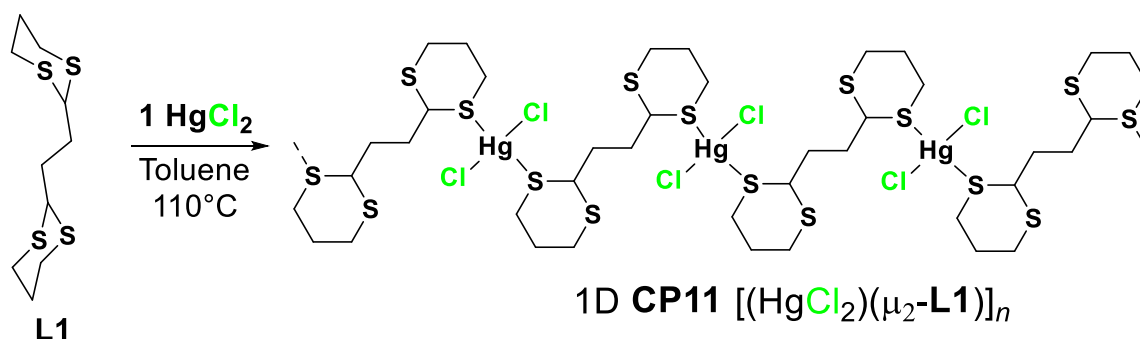


Figure 14. View of a segment of the 1D chain of $[\{\text{BrHg}(\mu_2\text{-Br})_2\text{HgBr}\}(\mu_2\text{-L1})]_n$ (**CP9**). The H atoms are omitted for clarity. Selected bond lengths (Å) and angles (°) at 100 K: Hg–S1 2.5456(8), Hg–Br1 2.5519(3), Hg–Br1# 3.0634(4), Hg–Br2 2.5383(4); S1–Hg–Br1 136.08(2), S1–Hg–Br1# 78.929(19), S1–Hg–Br2 111.05(2), Br1–Hg–Br2 112.750(12), Br1#–Hg–Br2 114.645(11), Br1–Hg–Br1# 85.973(102). Symmetry transformations used to generate equivalent atoms: ¹1-*x*, +*y*, 1/2-*z*; ²-*x*, 1-*y*, 1-*z*.

Reaction of **L1** with HgCl_2

A 1D polymer featuring an architecture very similar to that of **CP8** was formed upon coordination of **L1** on HgCl_2 in hot toluene (Scheme 6). Unfortunately, the poor

crystallographic quality of the colourless needles of the crystal structure shown in Fig. 15 does not allow a detailed discussion of the metric parameters. However, and in line with the elemental analysis, the data sets confirm without ambiguity the formation of a ribbon with composition $[(\text{HgCl}_2)(\mu_2\text{-L1})]_n$, (**CP11**) in which tetrahedral HgCl_2 units are linked through bridging **L1** ligands. The PXRD pattern also confirms the purity of the sample (Fig. S18).



Scheme 6. Synthesis of **CP11**.

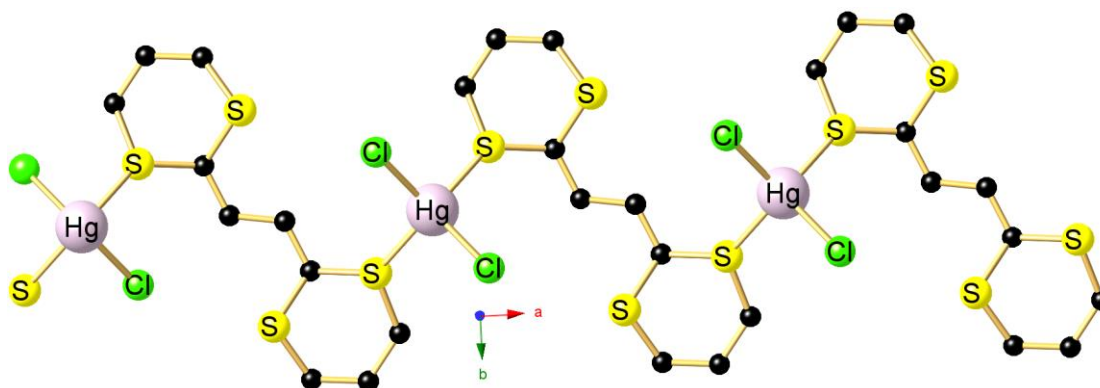
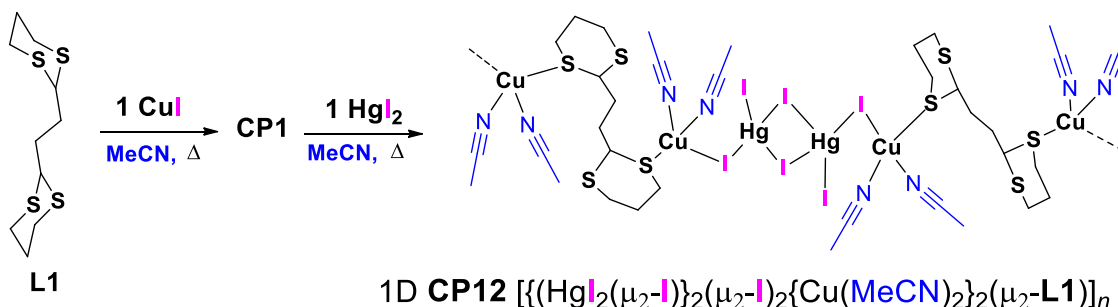


Figure 15. View of a segment of the 1D chain of $[(\text{HgCl}_2)(\mu_2\text{-L1})]_n$ (**CP11**). The H atoms are omitted for clarity.

Reaction of CP1 with HgI2

The fact that the network of $[\{\text{Cu}(\mu_2\text{-I})_2\text{Cu}\}(\mu_2\text{-L1})_2]_n$ (**CP1**) incorporates two non-coordinated sulphur atoms per **L1** ligand, potentially available as donor sites for complexation of further metal centres, intrigued us to probe the construction of heterometallic networks. With this objective in mind, we prepared first **CP1** *in situ* using hot acetonitrile as solvent (Scheme 7). After allowing to reach ambient temperature, one equivalent of HgI_2 was added to precipitated **CP1**. After stirring for 4h, an important part

of the suspended **CP1** had been dissolved as well as red HgI₂. The mixture was then heated to 80°C for one hour giving a yellowish clear solution. After allowing to reach ambient temperature, the growth of yellow crystals commenced. After partial evaporation of the solvent, the crystals were collected and analysed by X-ray diffraction.



Scheme 7. Synthesis of the heterometallic 1D polymer **CP12**.

Figure 16 shows that the initial 2D network of **CP1** has been broken and instead a heterometallic 1D ribbon has been formed. The chain is constructed of tetranuclear $[\text{IHg}(\mu_2\text{-I})_2\text{HgI}(\mu_2\text{-I})\text{Cu}]$ blocks consisting of dimerized HgI₂ units interconnected by two $\mu_2\text{-I}$ atoms. The tetrahedral coordination sphere around each Hg atom is completed by one terminal iodo ligand. These centrosymmetric $\text{IHg}(\mu_2\text{-I})_2\text{HgI}$ block share furthermore a second bridging $\mu_2\text{-I}$ ligand with a Cu(I) atom, which bears two metal-bound MeCN ligands. The $\text{Hg}\cdots\text{Hg}$ and $\text{Hg}\cdots\text{Cu}$ separations of 3.394 and 3.991 Å exclude any intermetallic interactions.⁵⁸ These tetranuclear SBUs are linked through the S1 atoms of **L1**, generating thus a linear 1D ribbon. The Cu–S1 distance of 2.3005(7) Å is similar to the mean Cu–S bond lengths of 2.3003 Å encountered in **CP1**, all other metric parameters are presented in the caption of Figure 16. The parallel running arrangement of the ribbons of **CP12** in the packing is shown in Figure S10 and the PXRD pattern in Figure S19.

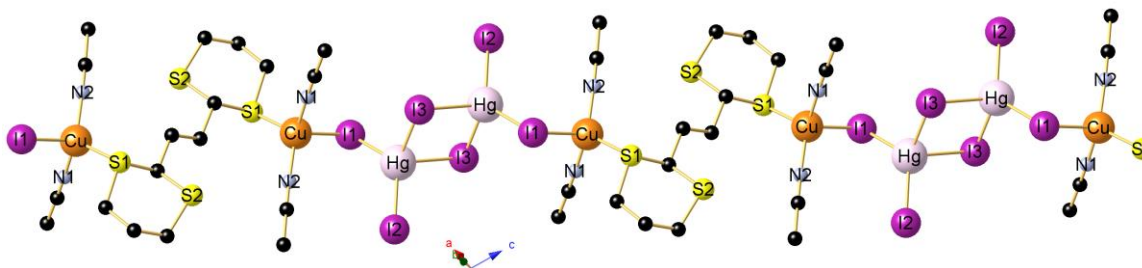


Figure 16. View of a segment of the heteronuclear 1D chain of $[\{\text{IHg}(\mu_2\text{-I})_2\text{HgI}(\mu_2\text{-I})_2\{\text{Cu}(\text{MeCN})_2\}_2(\mu_2\text{-L1})\}]_n$ (**CP12**) running along the *c* axis. The H atoms are omitted for clarity. Selected bond lengths (Å) and

angles (°) at 100 K: Hg–I1 2.7283(3), Hg–I2 2.6848(3), Hg–I3 3.0222(3), Hg–I3¹ 2.8429(3), I1–Cu 2.6731(4), Cu–S1 2.3005(7), Cu–N1 1.984(2), Cu–N2 1.964(2); I1–Hg–I3¹ 110.012(8), I1–Hg–I3 97.895(7), I2–Hg–I1 124.575(8), I2–H1–I3¹ 114.804(8), I3¹–Hg–I3 95.813(8), Cu1–I1–Hg 95.251(9), Hg¹–I3–Hg 84.187(8), S1–Cu–I1 99.411(18), N1–Cu–I1 107.18(7), N1–Cu–S1 109.68(7), N2–Cu–I1 108.34(7), N2–Cu–S1 117.13(7), N2–Cu–N1 113.70(9), Symmetry transformations used to generate equivalent atoms: ¹-x,1-y,2-z; ²1-x,2-y,1-z

The presence of two Cu-bound acetonitrile ligands indicated by elemental analysis is also confirmed by the IR spectrum of **CP12**, which exhibits two $\nu(\text{CN})$ vibrations at 2296 and 2267 cm^{-1} (Figure S21). Metal-bound MeCN ligands are often coordinated in a quite labile manner on a given metal center.^{59, 60} However, in the case of **CP12**, no degradation of the yellow crystals by dissociation of volatile MeCN was observed, even upon exposure to air for prolonged periods.

Although several other examples of mixed paramagnetic Cu(II)/Hg compounds featuring an $[\text{Cu}(\mu_2\text{-X})\text{Hg}(\mu_2\text{-X}_2\text{HgX}(\mu_2\text{-X})\text{Cu})]$ array like tetranuclear $[\text{Cu}(\text{bipy})_2\text{Hg}_2\text{Cl}_6]_2$ and 1D polymeric $[\text{Cu}_2(\text{bipy})_4\text{Hg}_2\text{Br}_6][\text{Hg}_4\text{Br}_{10}]$ are literature-known, an architecture as encountered for **CP12** is unprecedented.^{61, 62} The most reminiscent is that of $[(\mu\text{-}7,10,21,24\text{-tetraoxa-}4,13,18,27\text{-tetrathiatricyclo}[14.12.1.12,15]\text{triaconta-}1(29),2(30),15\text{-triene})\text{-hexakis}(\mu\text{-I})\text{-bis}(\text{MeCN})\text{-diiodo-tetra-copper(I)-di-mercury(II)},$ in which a macrocyclic tetrathioether ligand is coordinated through two S-donor sites to a CuI(MeCN) fragment, which in turn is linked to mononuclear Hg(II) centres via shared $\mu\text{-I}$ bridges (refcode JIBLEO).⁶³

Thermal properties

All compounds were found to be stable for several months under ambient atmosphere. Since the thermal stability is of crucial role for application in material sciences, that of the copper-based **CP1-CP6** has been measured under air flow in the temperature range 20–850°C. TGA traces are depicted in Figure 17 and the first derivative plots of the TGA traces are given in the Supporting Information (Figures S22–S27). Decomposition temperatures (corresponding to a 5% loss of the total mass) are compared to those obtained with **L2**-based CPs reported previously and are summarized in Table 1.²²

All CPs obtained with **L1**, except **CP5**, present high thermal stability with T_{dec} ranging from 232°C to 272°C. The thermal stability of **CP5** is the lowest ($T_{\text{dec}} = 150^\circ\text{C}$) due to the loss of coordinated acetonitrile. After that initial degradation step, the decomposition profile of **CP5** looks alike those obtained with others copper iodide-based CPs. The presence of $\text{Cu}(\mu_2\text{-I}_2)(\mu_2\text{-I}_4)\text{Cu}$ SBUs in **CP3** led to the highest thermal stability. As previously observed,^{22, 29} the decomposition profiles of **CP1**, **CP2** and **CP3** containing iodide present two well-defined decomposition steps while those of **CP4** and **CP5** containing bromide presents three main losses. The decomposition of **CP6** is even more complicated with at least four decomposition steps. This complicated decomposition profile led to an important difference between the theoretical and experimental values based on the ligand degradation (57% and 40%, respectively). However, for the other CPs, there is a good matching between the values. Finally, except for **CP6**, the final residues might be attributed to the formation of CuO as evidenced by comparison between theoretical and experimental values. Comparison of the thermal stabilities between the different CPs obtained from **L1** and **L2** shows that **L1**-based CPs present higher thermal stabilities. The higher stability found in the present paper for CPs obtained with **L1** might be attributed either to the fact that **L2** has a boiling point of 78°C while **L1** is a solid with melting point of 132-135°C or to the higher dimensionality obtained with **L1** (2D vs 1D) while having same SBUs (see for example comparison between the 2D **CP2** and the 1D CP $[\{\text{Cu}(\mu_2\text{-I})_2\text{Cu}\}(\mu_2\text{-L2})_2]_n$).

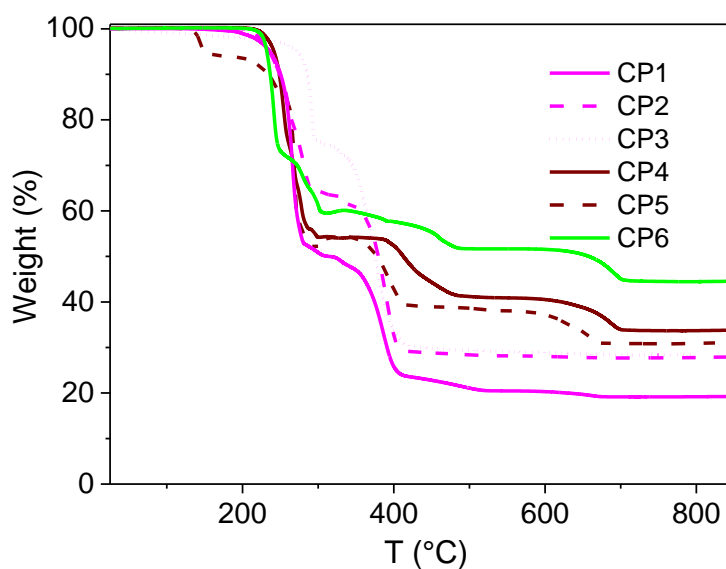


Figure 17. TGA traces of **CP1-CP6** under air flow (rate 10°C.min⁻¹)

Table 1. TGA data for **CP1-CP6**.

CP	T _{Dec} (°C)	T (°C)	Mass loss (% wt)		Residual mass (% wt)	
			Theo	Exp	Theo.	Exp
2D CP1 [$\{\text{Cu}(\mu_2\text{-I})_2\text{Cu}\}(\mu_2\text{-L1})_2\}_n$]	236	100-340	58 ^a	52	17 ^c	19
2D CP2 [$\{\text{Cu}(\mu_2\text{-I})_2\text{Cu}\}(\mu_4\text{-L1})_n$]	235	100-345	41 ^a	39	25 ^c	28
2D CP3 [$\{\text{Cu}(\mu_4\text{-I})(\mu_2\text{-I})\text{Cu}\}_2(\mu_4\text{-L1})_n$]	272	100-340	26	28	31	28
1D [$\{\text{Cu}(\mu_2\text{-I})_2\text{Cu}\}(\mu_2\text{-L2})_2\}_n$] ^d	160 ^d					
2D CP4 [$\{\text{Cu}(\mu_2\text{-Br})_2\text{Cu}\}(\mu_4\text{-L1})_n$]	241	100-350	46 ^a	48	29 ^c	34
1D [$\{\text{Cu}(\mu_2\text{-Br})_2\text{Cu}\}(\mu_2\text{-L2})_2\}_n$] ^d	187 ^d					
1D CP5 [$\{\text{Cu}(\mu_2\text{-Br})_3(\text{MeCN})(\mu_4\text{-L1})_{0.5}(\mu_5\text{-L1})_{0.5}\}_n$]	150	60-160	5.6 ^b	5.6		
		150-300	36 ^a	40	32 ^c	31
2D CP6 [$\{\text{Cu}(\mu_2\text{-Cl})_2\text{Cu}\}(\mu_4\text{-L1})_n$]	232	100-350	57 ^a	40	34 ^c	44
1D [$\{\text{Cu}(\mu_2\text{-Br})_2\text{Cu}\}(\mu_2\text{-L2})_2\}_n$] ^d	173 ^d					

^a values determined based on ligand loss

^b value determined based on CH₃CN loss

^c values determined based on the formation of CuO

^d data from ref [21]

Concluding Remarks and Perspectives

This investigation has shown that commercially available and inexpensive 2,2'-ethylenebis(1,3-dithiane) has, apart from its application as substrate in organic chemistry, also a promising potential as ligand in coordination chemistry. It may act, in function of the reaction conditions, both as tetradentate μ_4 - or bidentate μ_2 -type ligand, in which S-donor atoms behave as a 2-electron donor. However, the observation of a bridging S atom in **CP5** acting as a 4-electron donor demonstrates that, in contrast to tetradentate organophosphorous ligands, **L1** is even able to extend its coordination to a μ_5 -bonding mode. In the case of the complexation with Cu(I) salts, in all cases formation of stable coordination polymers is observed, but a rational control of the network architecture is a difficult task.^{7, 64} As already noticed in previous papers and by other research groups working on Cu(I) • thioether compounds, the outcome depends on too many factors like nature of the halide, metal-to-ligand ratio, reaction temperature, choice of the solvent, order of the addition of the reactants *etc.* But this unpredictability also opens the possibility to isolate and characterize hitherto unknown network architectures, as it is the case in the present study. Both **CP1** and **CP2** incorporate the very common rhomboid-shaped Cu(μ_2 -I)₂Cu motif as connecting nodes, but with very diverging Cu...Cu separations ranging from 2.6131(9) to 2.9436(5) Å underlying the structural flexibility of this SBU. **CP1** represents furthermore an unique case incorporating three crystallographically non-equivalent Cu(μ_2 -I)₂Cu SBUs. The 2D **CP3** obtained by increasing the CuI ratio features both μ_4 -type and μ_2 -type halide ligands.

The situation becomes even more curious in the case of CuBr. In both **CP4** and **CP5**, no Cu(μ_2 -Br)₂Cu SBUs are present, instead (–Cu–Br–Cu–Br–)_n chains are interconnected by μ_4 - or μ_5 -bridging **L1** ligands. The bonding situation within the 1D ribbon of [$\{Cu(\mu_2$ -Br)₃(MeCN)(μ_4 -**L1**)_{0.5}(μ_5 -**L1**)_{0.5}]_n (**CP5**) gets even more exotic since this compound features also metal-coordinated MeCN molecules and, as highlight, presents an extremely scarce case of a low-coordinate trigonal Cu center. So the nuclearity differs much of the simple 1D architecture of [$\{Cu(\mu_2$ -Br)₂Cu $\}(\mu_2$ -**L2**)₂]_n encountered with the structurally related 2-methyl-1,3-dithane **L2** ligand. With CuCl, a 2D network [$\{Cu(\mu_2$ -Cl)₂Cu $\}(\mu_4$ -**L1**)_n (**CP6**), at first glance, reminiscent to that of **CP2** is formed, however the very loose

Cu...Cu contact of 3.147 Å underpins the high structural flexibility of the Cu(μ_2 -X)₂Cu motifs. As expected from the use of this tetrathioether ligand **L1**, the dimensionality of the resulting CPs was increased from 1D to 2D compared to those obtained with **L2**. Unfortunately, probably due to the steric hindrance in **L1**, we failed to isolate MOF-like 3D networks incorporating strongly luminescent polynuclear (CuI)_n (n = 4, 6, 8) cluster as obtained with **L2** and other dithioether ligands.^{13, 21, 28, 65, 66}

Although we did not investigate in depth the coordination chemistry of **L1** and **L2** towards HgX₂ salts, we have evidenced that the composition of the resulting compounds can be influenced by the HgX₂-to-**L** ratio and that the dimensionality remains invariably 1D for **L1**. In contrast, reaction of **L2** with HgI₂ and HgBr₂ may lead to formation of a discreet mono- or dinuclear complexes but may also give rise to a polymeric 1D chain. The fact that in sulphur-rich **CP1** every second S atom is not engaged in dative M-S bonding has been successfully exploited to construct the heterometallic material [$\{ \text{IHg}(\mu_2\text{-I})_2\text{HgI}(\mu_2\text{-I})_2\{ \text{Cu}(\text{MeCN})_2\}_2(\mu_2\text{-L1}) \}_n$] (**CP12**) by addition of HgI₂. Several other compounds such as **CP7**, **CP8**, **D1** and **M1** also bear such potential S-donor sites. This feature opens the possibility for forthcoming work to construct systematically heterometallic assemblies by coordination of other ML_n fragments or MX_n salt, which may in turn serve as promising precursors for heterometallic sulphide phases and related materials.

EXPERIMENTAL SECTION

Materials and Apparatus

The CuX and HgX₂ salts, **L1** and **L2** were commercial obtained from Acros, Alfa Aesar and Aldrich. Infrared spectra were recorded with a 2 cm⁻¹ resolution on a Bruker vertex70 FTIR spectrometer using of a Platinum ATR accessory equipped with a diamond crystal. Thermogravimetric analysis (TGA) was carried out on a TA Instruments Q600 in an alumina crucible under an air flow with a heating rate of 10 °C min⁻¹ up to 850 °C.

Syntheses

CP1. To a solution a solution of CuI (191 mg, 1.0 mmol) in acetonitrile (20 mL) was added **L1** (271.5 mg, 1.02 mmol) in two portions.). Precipitation of a white product occurred immediately. The mixture was stirred for 2h at room temperature, and then heated to reflux

for 5 min to assure completion of the reaction. After reaching ambient temperature, the resulting microcrystalline precipitate was filtered off and air-dried. Yield (89%). To obtain X-ray suitable single-crystals, a 100 mg amount was redissolved in boiling MeCN and then allowed to reach slowly ambient temperature. mp = 272°C IR (ATR): 2931, 2900, 2826, 1427, 1410, 1307, 1272, 1252, 1237, 1177, 1134, 1108, 1028, 995, 906, 871, 829, 787, 756, 734, 678, 657, 616, 489, 421 cm⁻¹. Anal. Calc. for C₁₀H₁₈CuIS₄ (456.96): C, 26.28; H, 3.97; S, 28.07. Found: C, 26.46; H, 3.95; S, 27.93 %.

CP2. L1 (271.5 mg, 1.02 mmol) was dissolved in a mixture of acetonitrile (30 mL) and dichloromethane (5 mL). To this solution was added a solution of CuI (388 mg, 2.03 mmol) in acetonitrile (20 mL). Precipitation of a white product occurred immediately. The mixture was stirred 2h at room temperature. The resulting precipitate was filtered and washed with 20 mL of acetonitrile and then 20 mL of dichloromethane. Yield: 80%. A small amount of the white powder was dissolved in hot acetonitrile. After two weeks, colourless crystals suitable for single X-ray diffraction were obtained. mp = 232°C. IR (ATR): 2969, 2919, 1409, 1277, 1245, 1186, 1148, 1106, 1089, 983, 953, 850, 726, 691, 670, 468 cm⁻¹. Anal. Calc. for C₁₀H₁₈Cu₂I₂S₄ (647.36): C, 18.55; H, 2.80; S, 19.81. Found: C, 18.91; H, 2.80; S, 19.58%.

CP3. L1 (279.5 mg, 1.05 mmol) was dissolved in a mixture of acetonitrile (10 mL) and dichloromethane (5 mL). To this solution was added a solution of CuI (900 mg, 4.72 mmol) in acetonitrile (40 mL). Precipitation of a white product occurred immediately. The mixture was stirred 2h at room temperature. The resulting precipitate was filtered and washed with 20 mL of acetonitrile and then 20 mL of dichloromethane. Yield: 88%. Crystals suitable for X-Ray diffraction were obtained by slow diffusion of a dichloromethane solution of L1 into an acetonitrile solution of CuI (ratio ligand/metal 1:4) at room temperature. mp = 281°C. IR (ATR): 2941, 2926, 2893, 2831, 1421, 1339, 1315, 1284, 1240, 1188, 1136, 1032, 1002, 906, 872, 832, 790, 676, 655, 624, 429 cm⁻¹. Anal. Calc. for C₁₀H₁₈Cu₄I₄S₄ (1028.31): C, 11.68; H, 1.76; S, 12.47. Found: C, 11.96; H, 1.76; S, 12.13%.

CP4. To a solution of CuBr (287 mg, 2.0 mmol) in acetonitrile (16 mL) was added **L1** (266.5 mg, 1.0 mmol) in two portions.). Precipitation of a white product occurred

immediately. The mixture was stirred for 2h at room temperature, and then heated to reflux for 5 min to assure completion of the reaction. After reaching ambient temperature, the resulting microcrystalline precipitate was filtered off and air-dried. Yield (92%). To obtain X-ray suitable single-crystals, a 100 mg amount was redissolved in boiling EtCN and then allowed to reach slowly ambient temperature. mp = 244°C IR (ATR): 2988, 2892, 1421, 1342, 1276, 1242, 1214, 1189, 1157, 1125, 1051, 1011, 991, 925, 902, 863, 833, 773, 743, 676, 649, 601, 506, 486, 463; 429 cm⁻¹. Anal. Calc. for C₁₀H₁₈Cu₂Br₂S₄(553.41): C, 21.70; H, 3.28; S, 23.18. Found: C, 21.75; H, 3.25; S, 22.62%.

CP5. L1 (125 mg, 0.5 mmol) was dissolved in dichloromethane (5 mL). To this solution was added a solution of CuBr (208 mg, 1.45 mmol) in acetonitrile (25 mL). Precipitation of a white product occurred immediately. The mixture was stirred 2h at room temperature. The resulting precipitate was filtered and washed with 20 mL of acetonitrile and then 20 mL of dichloromethane. A small amount of the white powder was dissolved in hot acetonitrile. After two weeks, colourless crystals suitable for single X-ray diffraction were obtained. Yield: 75 %. mp = 236°C IR (ATR): 2972, 2933, 2910, 2837, 2309, 2265, 1433, 1408, 1376, 1344, 1274, 1259, 1244, 1209, 1187, 1174, 1162, 1033, 1010, 923, 897, 869, 856, 832, 775, 668, 646, 602, 482, 464, 421 cm⁻¹. Anal. Calc. for C₂₄H₄₂Br₆Cu₆N₂S₈ (1475.77): C, 19.53; H, 2.87; N, 1.90, S, 17.38. Found: C, 19.74; H, 2.90; N, 1.94; S, 16.97%

CP6. To a solution of CuCl (200 mg, 2.0 mmol) in acetonitrile (15 mL) was added solid **L1** (271.5 mg, 1.02 mmol) in three portions. Precipitation of a white product occurred immediately. The mixture was stirred 2h at room temperature. The resulting precipitate was filtered off, washed with 5 mL of acetonitrile and dried. Yield: 93%. A 100 mg amount of this material was dissolved in hot benzylocyanide. Upon cooling, colourless crystals suitable for X-ray diffraction were obtained. mp = 215°C. IR (ATR): 2941, 2906, 1447, 1421, 1311, 1267, 1229, 1181, 1160, 1106, 1027, 896, 874, 827, 798, 742, 687, 654, 438 cm⁻¹. Anal. Calc. for C₅H₉ClCuS₂ (232.23): C, 25.86; H, 3.91; S, 27.61. Found: C, 26.28; H, 4.20; S, 26.69.

CP7. To a suspension of HgI₂ (227 mg, 0.50 mmol) in toluene (10 mL) was added solid **L1** (271.5 mg, 1.02 mmol) in two portions. After stirring for 30 min, the mixture was heated to 110° C to give a clear solution. After 2h, the heating was stopped, and pale-yellowish

crystals started to grow upon cooling. After 2d, the supernatant toluene solution was decanted, and the stable crystals air-dried. Partial evaporation of the toluene solution afforded a further crop of **CP7**. Yield: 85%. mp = 148°C. IR (ATR): 2979, 2900, 1408, 1304, 1242, 1169, 1124, 1061, 897, 865, 784, 730, 653, 482 cm⁻¹. Anal. Calc. for C₁₀H₁₈HgI₂S₄ (720.87): C, 16.66; H, 2.51; S, 17.79. Found: C, 16.75; H, 2.49; S, 17.67 %.

D1. To a suspension of HgI₂ (227 mg, 0.50 mmol) in toluene (10 mL) was added **L2** (74 mg, 0.55 mmol) via syringe (66 µL). After stirring for 30 min, the mixture was heated to 110° C to give a clear solution. After 2h, the heating was stopped, and large yellow crystals were grown upon cooling. After 2d, the supernatant toluene solution was decanted, and the stable product air-dried. Partial evaporation of the toluene solution afforded a further crop of crystalline **D1**. Yield: 92%. mp = 113 °C. IR (ATR): 2925, 2895, 2824, 1438, 1416, 1374, 1341, 1274, 1236, 1190, 1119, 1076, 1053, 993, 973, 896, 859, 818, 713, 669, 645, 622, 479, 436 cm⁻¹. Anal. Calc. for C₁₀H₂₀HgI₂S₄ (1177.28): C, 10.20; H, 1.71; S, 10.89. Found: C, 10.39; H, 1.72; S, 10.97 %.

CP8. To a suspension of HgBr₂ (360 mg, 1.0 mmol) in toluene (10 mL) was added solid **L1** (271.5 mg, 1.02 mmol). After stirring for 30 min, the mixture was heated to 110° C to give a clear solution. After 2h, the heating was stopped, and colourless crystals commenced to grown upon cooling. After 2 days, the supernatant toluene solution was decanted, and the stable crystals air-dried. Partial evaporation of the toluene solution afforded a further small crop of **CP8**. Yield: 68%. mp = 170° C. IR (ATR): 2954, 2926, 2901, 2819, 1430, 1419, 1403, 1308, 1271, 1237, 1165, 1130, 1109, 1023, 904, 870, 828, 795, 753, 727, 678, 654, 634, 489, 417 cm⁻¹. Anal. Calc. for C₁₀H₁₈Br₂HgS₄ (626.89): C, 19.16; H, 2.89; S, 20.46. Found: C, 20.50; H, 3.08; S, 21.66 %.

CP9. This colourless compound was prepared in a similar manner by heating a mixture of HgBr₂ (360 mg, 1.0 mmol) in toluene (12 mL) with **L1** (133.0 mg, 0.5 mmol). Yield: 76%. mp = 177° C. IR (ATR): 2965, 2898, 2824, 1451, 1414, 1323, 1260, 1240, 1177, 1109, 1071, 1050, 1041, 861, 830, 798, 722, 639, 436 cm⁻¹. Anal. Calc. for C₅H₉Br₂HgS₂ (493.65): C, 12.16; H, 1.84; S, 12.99. Found: C, 12.38; H, 1.84; S, 12.91 %.

M1. To a suspension of HgBr₂ (360 mg, 1.0 mmol) in toluene (12 mL) was added **L2** (295 mg, 2.2 mmol) via syringe. After stirring for 30 min, the mixture was heated to 110° C to

give a clear solution. After 2h, the heating was stopped, and fine colourless crystal needles were grown upon cooling. After 1d, the supernatant toluene solution was decanted, and the stable product air-dried. Partial evaporation of the toluene solution afforded a further crop of crystalline **M1**. Yield: 86%. mp = 105 °C. IR (ATR): 2965, 2950, 2909, 1442, 1433, 1422, 1399, 1379, 1345, 1270, 1257, 1231, 1171, 1115, 1075, 1051, 996, 973, 900, 863, 813 cm^{-1} .

CP10. To a suspension of **M1** (126 mg, 0.2 mmol) in toluene (8 mL) was added HgBr_2 (72 mg, 0.2 mmol). After stirring for 30 min, the mixture was heated to 110° C to give a clear solution. After 1h, the heating was stopped, and large transparent crystals were grown upon cooling. After 1d, the supernatant toluene solution was decanted, and the stable product air-dried. Yield: 86%. mp = 112 °C. IR (ATR): 2967, 2934, 2910, 1449, 1424, 1398, 1337, 1249, 1231, 1165, 1116, 1077, 1057, 999, 968, 901, 864, 812 cm^{-1} . Anal. Calc. for $\text{C}_5\text{H}_{10}\text{HgBr}_2\text{S}_2$ (494.66): C, 12.14; H, 2.04; S, 12.96. Found: C, 12.47; H, 2.07; S, 13.46 %.

CP11. This compound was prepared in a similar manner as described for **CP8** by heating a 1:1 mixture of **L1** and HgCl_2 in toluene. Yield: 73%. mp = 160°C. IR (ATR): 2964, 2902, 2859, 1453, 1415, 1325, 1264, 1242, 1178, 1115, 1033, 1003, 899, 862, 833, 803, 728, 674, 642, 564, 504 cm^{-1} . Anal. Calc. for $\text{C}_{10}\text{H}_{18}\text{Cl}_2\text{HgS}_4$ (538.01): C, 22.32; H, 3.37; S, 23.84. Found: C, 21.62; H, 3.24; S, 22.77 %.

CP12. To a solution a solution of CuI (191 mg, 1.0 mmol) in acetonitrile (20 mL) was added **L1** (271.5 mg, 1.0 mmol) in two portions. After precipitation of a *in situ* generated **CP1**, the slurry was stirred for 1h at room temperature, and then heated to 80 C° for 15 min to assure completion of the reaction. After cooling ambient temperature, red HgI_2 (454 mg, 1.0 mmol) was added in two portions. Dissolution of HgI_2 occurred rapidly and an important part of **CP1** went in solution. After stirring for 4h, the mixture was heated for 10 min to give a clear yellowish solution. Upon cooling, yellow crystals formed progressively. The solvent volume was reduced to 15 ml by partial evaporation from the opened Schlenk flask. Yield: 67%. A further crop of **CP12**, contaminated by small amounts of **CP7**, was obtained by storing the solution in a refrigerator. mp = 110°C. IR (ATR): 2979, 2955, 2940, 2907, 2852, 2821, 2295, 2267, 1446, 1413, 1357, 1313, 1274, 1256, 1239, 1177, 1139, 1023, 903, 863,

831, 795, 744, 678, 658, 494, 421 cm⁻¹. Anal. Calc. for C₉H₁₅CuHgI₃N₂S₄ (860.21): C, 12.56; H, 1.75; N, 3.25; S, 7.45. Found: C, 12.84; H, 1.77; N, 3.19; S, 7.74 %.

X-ray Crystallography

X ray powder patterns were obtained at 295 K on a D8 Advance Bruker diffractometer using Ni-filtered K- α radiation. The crystal structures of the compounds **L1**, **CP1**, **CP2**, **CP3**, **CP4**, **CP5**, **CP6**, **D1**, **CP7**, **CP8**, **M1**, **CP9**, **CP11** and **CP12** were determined using the *Bruker D8 Venture* four-circle diffractometer equipped with a *PHOTON II* CPAD detector by *Bruker AXS GmbH*. The X-ray radiation was generated by the *I μ S* microfocus source Mo (λ = 0.71073 Å) from *Incoatec GmbH* equipped with HELIOS mirror optics and a single-hole collimator by *Bruker AXS GmbH*. The crystals were covered with an inert oil (perfluoropolyalkyl ether) and mounted on the *MicroMount*, *MicroGripper* or *MicroLoop* from *MiTeGen*. The APEX 3 Suite (v.2019.1-0) software integrated with SAINT (integration) and SADABS (adsorption correction) programs by *Bruker AXS GmbH* were used for data collection. The processing and finalization of the crystal structure were performed using the Olex2 program.⁶⁷ The crystal structures were solved by the ShelXT structure solution program using the Intrinsic Phasing option, which were further refined by the ShelXL refinement package using Least Squares minimization.^{68, 69} The non-hydrogen atoms were anisotropically refined. The C-bound H atoms were placed in geometrically calculated positions, and a fixed isotropic displacement parameter was assigned to each atom according to the riding-model: C–H = 0.98–1.00 Å with $U_{\text{iso}}(\text{H}) = 1.5U_{\text{eq}}(\text{CH}_3)$ and $1.2U_{\text{eq}}(\text{CH})$ for other hydrogen atoms. The crystallographic data and structural refinement are listed in ESI in Tables S1-S7. The crystallographic data for the structures **L1**, **CP1**, **CP2**, **CP3**, **CP4**, **CP5**, **CP6**, **D1**, **CP7**, **CP8**, **M1**, **CP9**, **CP10** and **CP12** have been published as supplementary publication number 2060086(**L1**), 2060098 (**CP1**), 2060088 (**CP2**), 2105375 (**CP3**), 2060084 (**CP4**), 2060105 (**CP5**), 2060085 (**CP6**), 2060101 (**CP7**), 2060104 (**D1**), 2060108 (**CP8**), 2060103 (**CP9**), 2060110 (**M1**), 2060111 (**CP10**), 2105376 (**CP12**) the Cambridge Crystallographic Data Centre. A copy of these data can be obtained for free by with applying to CCDC, 12 Union Road, Cambridge CB2 IEZ, UK, fax: 144-(0)1223-336033 or e-mail: deposit@ccdc.cam.ac.uk.

Conflicts of interest

There are no conflicts to declare.

Acknowledgements

We are grateful to the CNRS and the Ministère de la Recherche et Technologie for financial support. We warmly thank Ms. V. Moutarlier for her help with the powder X-ray measurements. C. Strohmman, L. Brieger and L. Knauer thank the Deutsche Forschungsgemeinschaft *DFG* for financial support and the Fonds der Chemischen Industrie (*FCI*) for scholarships awarded to L. Knauer and L. Brieger.

Footnote

Electronic supplementary information (ESI) available: summary of X-ray data collection and refinement for all structures studied, structure views of **CP1-CP6**, **CP8-CP10**, powder X-Ray Patterns of **CP1-CP4**, **CP6-CP8**, **CP11-12**, ATR-IR spectra of **CP5**, **CP12**, TGA traces of **CP1-CP6**.

References

1. A. Schlachter and P. D. Harvey, *J. Mater. Chem. C*, 2021, **9**, 6648-6685.
2. J. Conesa-Egea, F. Zamora and P. Amo-Ochoa, *Coord. Chem. Rev.*, 2019, **381**, 65-78.
3. X. Guo, C. Huang, H. Yang, Z. Shao, K. Gao, N. Qin, G. Li, J. Wu and H. Hou, *Dalton Trans.*, 2018, **47**, 16895-16901.
4. T. H. Kim, H. Yang, G. Park, K. Y. Lee and J. Kim, *Chemistry – An Asian Journal*, 2010, **5**, 252-255.
5. S.-Q. Bai, I. H. K. Wong, N. Zhang, K. Lin Ke, M. Lin, D. J. Young and T. S. A. Hor, *Dalton Trans.*, 2018, **47**, 16292-16298.
6. Y. Liu, H. Peng, P. Wu, H. Liu and J. Zhang, *Polymer*, 2019, **179**, 121616.
7. A. Schlachter, K. Tanner and P. D. Harvey, *Coord. Chem. Rev.*, 2021, **448**, 214176.
8. H. W. Yim, L. M. Tran, E. E. Pullen, D. Rabinovich, L. M. Liable-Sands, T. E. Concolino and A. L. Rheingold, *Inorg. Chem.*, 1999, **38**, 6234-6239.

9. N. R. Brooks, A. J. Blake, N. R. Champness, P. A. Cooke, P. Hubberstey, D. M. Proserpio, C. Wilson and M. Schröder, *J. Chem. Soc., Dalton Trans.*, 2001, 456-465.
10. J. Y. Lee, S. Y. Lee, W. Sim, K.-M. Park, J. Kim and S. S. Lee, *J. Am. Chem. Soc.*, 2008, **130**, 6902-6903.
11. Y. Bi, W. Liao, X. Wang, R. Deng and H. Zhang, *Eur. J. Inorg. Chem.*, 2009, **2009**, 4989-4994.
12. Y.-C. Yang, S.-T. Lin and W.-S. Chen, *J. Chem. Res.*, 2008, **2008**, 280-284.
13. A. Raghuvanshi, C. Strohmann, J.-B. Tissot, S. Clément, A. Mehdi, S. Richeter, L. Viau and M. Knorr, *Chem. Eur. J.*, 2017, **23**, 16479-16483.
14. H. N. Peindy, F. Guyon, M. Knorr, A. B. Smith, J. A. Farouq, S. A. Islas, D. Rabinovich, J. A. Golen and C. Strohmann, *Inorg. Chem. Commun.*, 2005, **8**, 479-482.
15. H. Chiang, C. J. Moon, E. Kwon, H. Park, H. Im, M. Y. Choi, T. H. Kim and J. Kim, *Bull. Korean Chem. Soc.*, 2018, **39**, 1139-1143.
16. K. M. Henline, C. Wang, R. D. Pike, J. C. Ahern, B. Sousa, H. H. Patterson, A. T. Kerr and C. L. Cahill, *Cryst. Growth Des.*, 2014, **14**, 1449-1458.
17. L. Brammer, C. S. Rodger, A. J. Blake, N. R. Brooks, N. R. Champness, J. W. Cunningham, P. Hubberstey, S. J. Teat, C. Wilson and M. Schroeder, *J. Chem. Soc., Dalton Trans.*, 2002, DOI: 10.1039/b205278b, 4134-4142.
18. J. M. Knaust and S. W. Keller, *CrystEngComm*, 2003, **5**, 459-465.
19. M. Knorr, F. Guyon, A. Khatyr, M. Allain, S. M. Aly, A. Lapprand, D. Fortin and P. D. Harvey, *J. Inorg. Organomet. Polym.*, 2010, **20**, 534-543.
20. A. Raghuvanshi, N. J. Dargallay, M. Knorr, L. Viau, L. Knauer and C. Strohmann, *J. Inorg. Organomet. Polym.*, 2017, **27**, 2000-3000.
21. A. Schlachter, L. Viau, D. Fortin, L. Knauer, C. Strohmann, M. Knorr and P. D. Harvey, *Inorg. Chem.*, 2018, **57**, 13564-13576.
22. A. Raghuvanshi, M. Knorr, L. Knauer, C. Strohmann, S. Boullanger, V. Moutarlier and L. Viau, *Inorg. Chem.*, 2019, **58**, 5753-5775.
23. L. Knauer, M. Knorr, L. Viau and C. Strohmann, *Acta Crystallogr. E*, 2020, **76**, 38-41.

24. D. Seebach, N. R. Jones and E. J. Corey, *J. Org. Chem.*, 1968, **33**, 300-305.
25. R. A. Ellison and W. D. Woessner, *J. Chem. Soc., Chem. Commun.*, 1972, DOI: 10.1039/C39720000529, 529-530.
26. H. T. Kalff and C. Romers, *Acta Crystallogr. Sect. A*, 1966, **20**, 490-496.
27. A. Bonnot, M. Knorr, C. Strohmann, C. Golz, D. Fortin and P. Harvey, *J. Inorg. Organomet. Polym.*, 2015, **25**, 480-494.
28. A. Schlachter, A. Lapprand, D. Fortin, C. Strohmann, P. D. Harvey and M. Knorr, *Inorg. Chem.*, 2020, **59**, 3686-3708.
29. A. Bonnot, M. Knorr, F. Guyon, M. M. Kubicki, Y. Rousselin, C. Strohmann, D. Fortin and P. D. Harvey, *Cryst. Growth Des.*, 2016, **16**, 774–788.
30. T. H. Kim, H. Yang, G. Park, K. Y. Lee and J. Kim, *Chem. - Asian J.*, 2010, **5**, 252-255.
31. O. Veselska, D. Podbevšek, G. Ledoux, A. Fateeva and A. Demessence, *Chem. Commun.*, 2017, **53**, 12225-12228.
32. J. Troyano, Ó. Castillo, P. Amo-Ochoa, J. I. Martínez, F. Zamora and S. Delgado, *CrystEngComm*, 2019, **21**, 3232-3239.
33. M. Sakakibara, Y. Yonemura, Z. Tanaka, S. Matsumoto, K. Fukuyama, H. Matsuura and H. Murata, *J. Mol. Struct.*, 1980, **69**, 53-58.
34. L. Vigo, P. Salin, R. Oilunkaniemi and R. S. Laitinen, *Acta Crystallogr. E*, 2008, **E64**, m809
35. G. Singh, S. Bali, A. K. Singh, J. E. Drake, C. L. B. Macdonald, M. B. Hursthouse and M. E. Little, *Inorg. Chim. Acta*, 2005, **358**, 912-918.
36. Y. C. Cui, G. B. Che, X. F. Lin and C. B. Liu, *Acta Crystallogr. E*, 2006, **E62**, m1595-m1596.
37. G. B. Che, C. B. Liu, Y. C. Cui and C. B. Li, *Acta Crystallogr. E*, 2005, **E61**, m2704-m2705.
38. Q. Yu, Y. Tao and J.-R. Li, *Acta Crystallographica Section E*, 2006, **62**, m613-m614.
39. J. B. Gong, L. N. Zhou and W. Chen, *Acta Crystallogr. E*, 2006, **E62**, m440-m441.
40. M. E. Carnes, N. R. Lindquist, L. N. Zakharov and D. W. Johnson, *Cryst. Growth Des.*, 2012, **12**, 1579-1585.

41. M. Knorr, H. N. Peindy, F. Guyon, H. Sachdev and C. Strohmann, *Z. Anorg. Allg. Chem.*, 2004, **630**, 1955-1961.
42. H. N. Peindy, F. Guyon, M. Knorr and C. Strohmann, *Z. Anorg. Allg. Chem.*, 2005, **631**, 2397 - 2400.
43. V. Bertini, F. Lucchesini, M. Pocchi and S. Alfei, *Tetrahedron*, 2005, **61**, 9519-9526.
44. X. Zhang, Y. Xu, P. Guo and X. Qian, *New J. Chem.*, 2012, **36**, 1621-1625.
45. S. Yang, W. Yang, Q. Guo, T. Zhang, K. Wu and Y. Hu, *Tetrahedron*, 2014, **70**, 8914-8918.
46. M. H. Habibi, S. Tangestaninejad, M. Montazerzohori and I. Mohamadpoor-Baltork, *Molecules*, 2003, **8**, 663-669.
47. J. A. W. Dalziel, M. J. Hitch and S. D. Ross, *Spectrochim. Acta, Part A*, 1969, **25**, 1055-1060.
48. R. Fragnals, N. Barba-Behrens and R. Contreras, *Spectrochim. Acta, Part A*, 1989, **45A**, 581-584.
49. C. G. Hartinger, A. A. Nazarov, V. Chevchenko, V. B. Arion, M. Galanski and B. K. Keppler, *Dalton Trans.*, 2003, 3098-3102.
50. K. Brodersen, G. Liehr and W. Rölz, *Z. Anorg. Allg. Chem.*, 1977, **428**, 166-172.
51. K. Brodersen, J. Hoffmann and R. Erdmann, *Z. Anorg. Allg. Chem.*, 1981, **482**, 217-225.
52. N. Galesic, M. Herceg and D. Sevdic, *Acta Crystallogr. Sect. C*, 1986, **42**, 565-568.
53. J. Y. Lee, S. Lee, M. Jo, H. Lee, K. M. Park and S. S. Lee, *Bull. Korean Chem. Soc.*, 2009, **30**, 961 - 964.
54. S. J. Lee, J. H. Jung, J. Seo, I. Yoon, K.-M. Park, L. F. Lindoy and S. S. Lee, *Org. Lett.*, 2006, **8**, 1641-1643.
55. H. Müller, A. Kelling, U. Schilde and H.-J. Hold, *Z. Naturforsch., B: Chem. Sci.*, 2009, **64**, 1003-1015.
56. S. Chandrasekhar, D. Chopra, K. Gopalaiah and T. N. Guru Row, *J. Mol. Struct.*, 2007, **837**, 118-131.
57. X. Zhang, W. Yu, Y. Xie, Q. Zhao and Y. Tian, *Inorg. Chem. Commun.*, 2003, **6**, 1338-1340.

58. U. Bodensieck, P. Braunstein, M. Knorr, M. Strampfer, M. Bénard and C. Strohmann, *Angew. Chem. Int. Ed.*, 1997, **36**, 2758-2761.
59. G. Kang, Y. Jeon, K. Y. Lee, J. Kim and T. H. Kim, *Cryst. Growth Des.*, 2015, **15**, 5183-5187.
60. A. Schlachter, K. Tanner, R. Scheel, P.-L. Karsenti, C. Strohmann, M. Knorr and P. D. Harvey, *Inorg. Chem.*, 2021, DOI: 10.1021/acs.inorgchem.1c01856, 13528-13538.
61. D. B. Leznoff, N. D. Draper and R. J. Batchelor, *Polyhedron*, 2003, **22**, 1735-1743.
62. J.-L. Song, J.-G. Mao, H.-Y. Zeng and Z.-C. Dong, *Eur. J. Inorg. Chem.*, 2004, **2004**, 538-543.
63. S. Kim, A. D. Siewe, E. Lee, H. Ju, I.-H. Park, J. H. Jung, Y. Habata and S. S. Lee, *Cryst. Growth Des.*, 2018, **18**, 2424-2431.
64. P. D. Harvey and M. Knorr, *Journal of Inorganic and Organometallic Polymers and Materials*, 2016, **26**, 1174-1197.
65. J. Y. Lee, S. Y. Lee, W. Sim, K.-M. Park, J. Kim and S. S. Lee, *J. Am. Chem. Soc.*, 2008, **130**, 6902-6903.
66. M. Knorr, F. Guyon, A. Khatyr, C. Daeschlein, C. Strohmann, S. M. Aly, A. S. Abd-El-Aziz, D. Fortin and P. D. Harvey, *Dalton Trans.*, 2009, 948-955.
67. O. V. Dolomanov, L. J. Bourhis, R. J. Gildea, J. A. K. Howard and H. Puschmann, *J. Appl. Crystallogr.*, 2009, **42**, 339-341.
68. G. Sheldrick, *Acta Crystallogr. Sect. A*, 2015, **71**, 3-8.
69. G. Sheldrick, *Acta Crystallogr. Sect. C*, 2015, **71**, 3-8.